LM-06K005
February 15, 2006

An Experimental Investigation of the Structural Wave Scattering Due to Impedance Discontinuities on a Cylindrical Structure

RJ Glotzbecker

The Pennsylvania State University

The Graduate School

Graduate Program in Acoustics

AN EXPERIMENTAL INVESTIGATION OF THE STRUCTURAL WAVE SCATTERING DUE TO IMPEDANCE DISCONTINUITES ON A CYLINDRICAL STRUCTURE

A Paper in

Acoustics

by

Ryan Joseph Glotzbecker

Submitted in Partial Fulfillment
of the Requirements
for the Degree of

Master of Engineering in Acoustics

May 2006

Ryan Joseph Glotzbecker

The thesis of Ryan Joseph Glotzbecker was reviewed and approved* by the following:

Dr. Stephen A. Hambric
Head, Structural Acoustics Department
Applied Research Lab/ Pennsylvania State University
Thesis Advisor

Dr. John Fahnline
Research Associate
Applied Research Lab/ Pennsylvania State University

Dr. Anthony Atchley
Head, Graduate Program in Acoustics
Pennsylvania State University

*Signatures are on file in the Graduate School

ABSTRACT

Experimental, numerical, and analytical work has shown that the response of a shell to a distributed force wave possesses unique characteristics which are dependent on the nature of structure attached to the shell. Specific characteristics which influence the response are the distribution of the discontinuities around the circumference (periodic/a-periodic), the impedance of the discontinuities relative to that of the shell, and the type of impedance (mass or stiffness). Traditional shell theory predicts low frequency, radial-dominated structural mode shapes of a shell with a sinusoidal distribution of displacement amplitudes. Due to the orthogonal nature of these mode shapes, the response of the structure to a traveling radial force wave with sinusoidal content at a given harmonic is due solely to the response of the mode shape with harmonic content of the same order.

Introduction of impedance discontinuities to a shell yield complex mode shapes, which may be characterized by the summation of several harmonic components. These modes are no longer orthogonal in the presence of discontinuities, yielding harmonic content across various modal orders. As a result, a purely sinusoidal forcing function can excite several modes of the structure. Structural scattering as discussed in this paper refers to the phenomena in which a force wave at a given harmonic scatters into the response of modes with different harmonics. An experimental investigation into the harmonic scattering behavior of a shell due to mass discontinuities is presented in this paper. Knowledge of the key structural characteristics which influence scattering and

their behavior will allow for a diagnostic tool when assessing the structural response of more complex cylindrical structures.

Experimentally obtained data presented in this paper demonstrates some expected scattering characteristics of a cylindrical shell in the presence of periodically and a-periodically distributed masses. Some unique characteristics of the response of a shell in the presence of periodically distributed masses are discussed. Additionally, the data demonstrates that scattering characteristics may exist in even the simplest cylindrical structures due to non-idealities in the structure or its boundary conditions.

TABLE OF CONTENTS

LIST OF SYMBOLS

U	Axial component of shell displacement at the midsurface
V	Radial component of shell displacement at the midsurface
W	Circumferential component of shell displacement at the midsurface
Z	Axial coordinate of the shell
ϕ	Angular coordinate of the shell
υ	Poisson's ratio
E	Modulus of elasticity
a	Inner shell radius
h	Shell thickness
c_p	Speed of sound
V_n	Amplitude of the radial shell deflection due to mode n
W_n	Amplitude of circumferential shell deflection due to mode n
n	Spatial harmonic, mode number
ω	Circular Frequency
Ω	Non dimensional frequency ($\omega a/c_p$)
f_n	Harmonic component n of the force input wave
n_f	Harmonic order of force wave
n_r	Harmonic order of response wave
θ_f	Angular location of the input force
θ_r	Angular location of the response

$H_{\theta f,\theta r}(f)$	Frequency response function of the acceleration at θ_r due to a force at θ_f.
$A_{\theta r}(f)$	Acceleration spectrum at θ_r
$[A(f,\theta_r)]$	Matrix of acceleration measurements, as a function of frequency and response location.
$[A(f,n_r)]$	Matrix of acceleration measurements as a function of spatial harmonic
$F_{\theta f}(f)$	Spectrum of the force input
$[H(f,\theta_f,\theta_r]$	Matrix of FRFs as a function of frequency, input force location, and response location
$[T_{tw}]$	Traveling wave transformation matrix
N	Maximum resolvable spatial harmonic
$A_{nf,nr}(f)$	Acceleration of harmonic n_r to a force input at n_f.
$[T_{sw}]$	Standing Wave transformation matrix
A_s	Sine component of the acceleration response
A_c	Cosine component of the acceleration response
$H_{s,s}$	Response of the sine component at a given harmonic due to the sine component of a force at a given harmonic
$H_{s,c}$	Response of the sine component at a given harmonic due to the cosine component of a force at a given harmonic
MIF	Modal Indicator Function

$\omega_{n,0}$	Natural frequency of a mode with a circumferential harmonic n and no axial variation
ω_{mn}	Natural frequency of a mode with a circumferential harmonic n and axial harmonic m

LIST OF FIGURES

LIST OF TABLES

Chapter 1

Introduction

Experimental, numerical, and analytical work has shown that the response of a shell to a distributed force wave possesses unique characteristics which are dependent on the nature of structure attached to the shell. Specific characteristics which influence the response are the distribution of the discontinuities around the circumference (periodic/a-periodic), the impedance of the discontinuities relative to that of the shell, and the type of impedance (mass or stiffness). Traditional shell theory predicts low frequency, radial-dominated structural mode shapes of a shell with a sinusoidal distribution of displacement amplitudes. Due to the orthogonal nature of these mode shapes, the response of the structure to a traveling radial force wave with sinusoidal content at a given harmonic is due solely to the response of the mode shape with harmonic content of the same order.

Introduction of impedance discontinuities to a shell yield complex mode shapes, which may be characterized by the summation of several harmonic components. These modes are no longer orthogonal in the presence of discontinuities, yielding harmonic content across various modal orders. As a result, a purely sinusoidal forcing function can excite several modes of the structure. Structural scattering as discussed in this paper refers to the phenomena in which a force wave at a given harmonic scatters into the response of modes with different harmonics. An experimental investigation into the harmonic scattering behavior of a shell due to mass discontinuities is presented in this

paper. Knowledge of the key structural characteristics which influence scattering and their behavior will allow for a diagnostic tool when assessing the structural response of more complex cylindrical structures.

1.1 Basic Theory on the Vibration of Shells

The continuous nature of the circumferential dimension of cylindrical shells facilitates the analysis of these structures on a spatial harmonic basis. To demonstrate this, the derivation of the mode shapes of a cylindrical shell is discussed below. Several forms of the equations of motion for cylindrical shells have been proposed in literature. Reference [3] reviews the differences between these formulations. The experiments presented in this paper focus of the deviations in the forced response of a shell from the theoretical formulations on a harmonic basis. The differences in equations of motion primarily affect the computation of the natural frequencies of the modes, not the mode shapes. Therefore, a simplified derivation of the mode shapes of a cylindrical shell will be described in this paper. This derivation is a summary of that found in Reference [4]. In deriving the basic equations of motion for a cylindrical shell, the following assumptions were listed:

1. The thickness of the shell is small relative to the radius (i.e. $h/a < 0.1$)
2. The displacement is small relative to the shell thickness
3. The transverse normal stress acting on planes parallel to the shell middle surface is negligible

4. The middle surface of the shell is not subject to elongation during shell deformation (Bending strain energy >> Membrane strain energy)

A cylindrical coordinate system for a shell is shown in Figure 1-1. Donnell's formulation for the equations of motion of a shell in this coordinate system is:

$$\begin{aligned}
&\frac{\partial^2 u}{\partial \theta^2}+\frac{1-\nu}{2a^2}\frac{\partial^2 u}{\partial \theta^2}+\frac{1+\nu}{2a}\frac{\partial^2 v}{\partial z \partial \theta}+\frac{\nu}{a}\frac{\partial w}{\partial z}-\frac{\ddot{u}}{c_p^2}=0,\\
&\frac{1+\nu}{2a}\frac{\partial^2 u}{\partial z \partial \theta}+\frac{1-\nu}{2}\frac{\partial^2 v}{dz^2}+\frac{1}{a^2}\frac{\partial^2 v}{\partial \theta^2}+\frac{1}{a^2}\frac{\partial w}{\partial \theta}-\frac{\ddot{v}}{c_p^2}=0,\\
&\frac{\nu}{a}\frac{\partial u}{\partial z}+\frac{1}{a^2}\frac{\partial v}{\partial \theta}+\frac{w}{a^2}+\beta^2\left(a^2\frac{\partial^4 w}{\partial z^4}+2\frac{\partial^4 w}{\partial z^2 \partial \theta^2}+\frac{1}{a^2}\frac{\partial^4 w}{\partial \theta^4}\right)+\frac{\ddot{w}}{c_p^2}-\frac{p_a\left(1-\nu^2\right)}{Eh}=0,\\
&\beta^2=\frac{h^2}{12a^2},
\end{aligned} \tag{1.1}$$

where *u, v,* and *w* correspond to the axial, radial, and circumferential components of the displacement, *z* and θ correspond to the axial and angular coordinates of the shell, υ is Poisson's ratio of the shell material, *E* is the modulus of elasticity of the shell, *a* is the inner radius of the shell, *h* is the thickness of the shell, c_p is the speed of sound in the shell material, and p_a represents loading normal to the surface of the shell. For a shell with free-free boundary conditions, it has been shown that inextensional theory yields accurate results. If it is assumed that the radial and circumferential components of the displacement are independent of the axial coordinate, a solution to the equations of motion is assumed:

$$\begin{aligned}
&u=0,\\
&v=V_n\sin(n\theta)e^{-i\omega t},\\
&w=W_n\cos(n\theta)e^{-i\omega t},
\end{aligned} \tag{1.2}$$

where V_n and W_n represent the amplitudes of the radial and circumferential components of the shell deflection, n is the harmonic order of the mode, ω is the circular frequency, and t represents time. The angular dependence of the modal deflection in Equation 1.2 may be expressed in complex exponential notation as:

$$\begin{aligned} u &= 0, \\ v &= \frac{V_n}{2i}\left(e^{in\theta} - e^{-in\theta}\right)e^{-i\omega t}, \quad . \\ w &= \frac{W_n}{2}\left(e^{in\theta} + e^{-in\theta}\right)e^{-i\omega t}, \end{aligned} \tag{1.3}$$

This alternative expression of the solution to the equations of motion demonstrates the equality between a standing wave field and the summation of positive and negative traveling waves. Figure 1-1 shows the shape of the $n_r = 4$ mode.

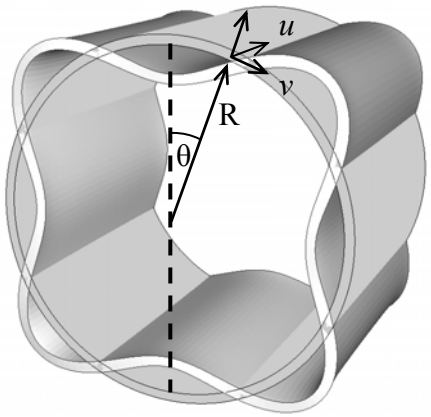

Figure 1-1: Cylindrical Shell Coordinate System, Deformation Directions, and $n_r = 4$ Mode Shape

The equations of motion for the free vibration (i.e. $p_a = 0$) of the shell may be rewritten as

$$\begin{bmatrix} n^2 - \Omega^2 & n \\ n & -\Omega^2 - \left(\beta^2 n^4\right) \end{bmatrix} \begin{Bmatrix} V_n \\ W_n \end{Bmatrix} = 0 \quad , \tag{1.4}$$

where the frequency is represented in non-dimensional form as $\Omega = \omega a / c_p$. The forced response of the shell may be found by replacing the right hand side of Equation 1.4 with the radial force distribution as shown:

$$\begin{bmatrix} n^2 - \Omega^2 & n \\ n & -\Omega^2 - \left(\beta^2 n^4\right) \end{bmatrix} \begin{Bmatrix} V_n \\ W_n \end{Bmatrix} = \begin{Bmatrix} 0 \\ -\dfrac{f_n a^2 \left(1 - \nu^2\right)}{Eh} \end{Bmatrix}, \tag{1.5}$$

where f_n is the harmonic component n of the force input wave. When the force input wave has a spatially sinusoidal shape ($\sin(n\theta)$), only the mode with harmonic order n is excited. Moreover, the radial displacement of the shell in response to a traveling wave force excitation at harmonic order n will be a wave at the same harmonic and traveling in the same direction as the force input. This characteristic allows for the analysis of test data on a spatial Fourier harmonic basis, where each Fourier component closely represents a single mode shape of the shell.

1.2 Theory on the Effects of Periodic Discontinuities

Early analytical work shown in Reference [3] attempted to account for the effect of periodic stiffeners around the circumference by distributing the added stiffness evenly around the shell. These approximations helped to show the effect that added impedance has on the natural frequency of the shell modes, but fails to account for the complexities

added to the actual deformation of the structure due to the added impedances. However, analyses by Schnell and Heinricshbauer, summarized in Reference [3], showed that two different types of modes are possible when internal stiffeners are evenly distributed around a shell. In one of the two modes, the stiffeners see little radial motion, and only twist with shell deflection. In this case, the impedance discontinuities are at the nodes of the radial deflection. In the second type of mode, the stiffeners see significant radial deflection, and therefore influence the natural frequency of the mode by changing the modal impedance. In this case, the impedance discontinuities are at the anti-nodes of the deflection. This mode-splitting phenomenon and the effects of complex mode shapes due to added impedance are explored experimentally later in this paper.

When periodic impedances are added to a structure, the naturally sinusoidal mode shape is transformed into a more complex mode shape, characterized by several Fourier harmonic components. As a result, when the structure with these complex mode shapes is excited by a force wave at a single harmonic, the response may consist of multiple harmonic orders. Literature on this subject is often found in two areas. First, the effect of the introduction of impedance discontinuities is often described in terms of the changes in the mode shape, as demonstrated in Reference [5]. The response of periodic structures to traveling waves is often discussed in terms of rotating structures, as demonstrated in References [6] and [7]. The concepts demonstrated in these two categories may be applied to a stationary shell with periodic impedance discontinuities, subjected to a traveling force wave. Reference [2] presents a finite element analysis of a shell with attached structure. The results of this study demonstrate that the response

harmonics n_r, excited by a force at harmonic n_f will be related to the number of periodically attached impedance discontinuities according to the following equation:

$$n_r = n_f \pm kZ \,, \tag{1.6}$$

where n_r is the harmonic order of the response wave, n_f is the harmonic order of the force wave, Z is the number of periodic impedance discontinuities, and k = [*1,2,3,...*]. Experimental results confirm the presence of this phenomenon as shown in Chapter 3.

1.3 Paper Overview

The remainder of this paper presents an experiment in which the scattering characteristics of a cylindrical shell are measured. Chapter 2 of this paper describes the experimental methods used to measure the scattering phenomena. The mathematical formulations used to post process the measured data into an intuitive form are also shown in this chapter. Chapter 3 discusses experimental results. This chapter discusses the measured characteristics of the basic shell response and the measured change in scattering characteristics when masses are attached to the outer circumference of the shell. The results for both periodically and a-periodically attached masses are presented. In Chapter 4, potential investigations for similar work in the future are presented.

Experimentally obtained data presented in this paper demonstrates some expected scattering characteristics of a cylindrical shell in the presence of periodically and a-periodically distributed masses. Some unique characteristics of the response of a shell in the presence of periodically distributed masses are discussed. Additionally, the data

demonstrates that scattering characteristics may exist in even the simplest cylindrical structures due to non-idealities in the structure or its boundary conditions.

Chapter 2

Measurement Procedures

2.1 Experimental Setup

The goal of the experiment presented in this paper is to demonstrate the changes in the response characteristics of an ideal cylindrical shell when impedance discontinuities are added. To accomplish this, the test was designed to be easily reconfigured while maintaining the integrity of the basic shell. Figure 2-1 shows a picture of the test setup where a pipe section is mounted vertically by resting on four pressurized rubber air springs. A description of this test setup including shell properties, boundary conditions, instrumentation, and data acquisition is discussed in this chapter.

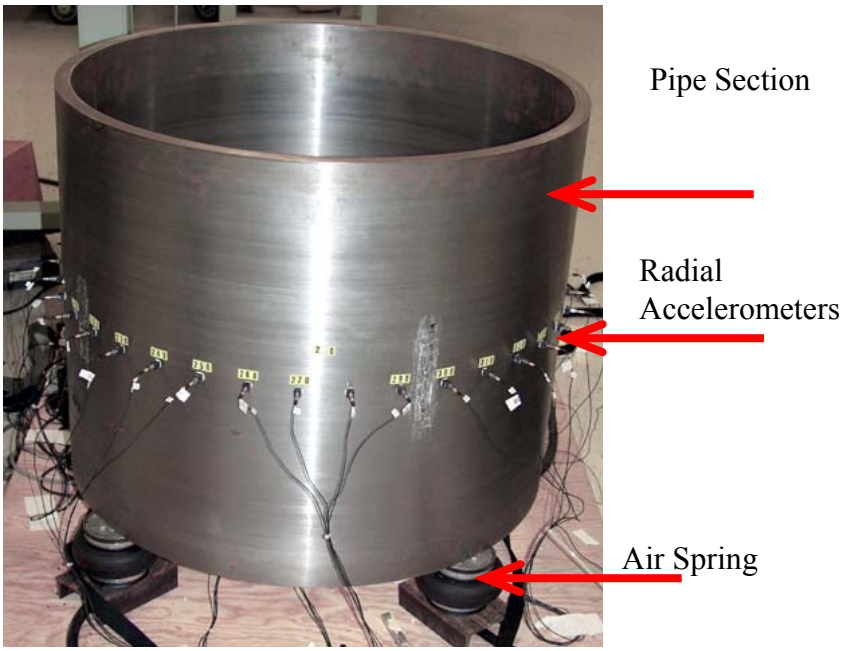

Figure 2-1: Picture of Test Setup

2.1.1 Shell Properties

A section of commercially available pipe was used for all of the experiments described in this paper. The pipe section used was a 24" (0.61m) long, 30" (0.76m) nominal O.D., 1" (0.025m) nominal wall thickness welded carbon steel pipe. To minimize the scattering effects of the weld seam, the pipe was machined to ensure a constant wall thickness and circular inner and outer diameters. After the machining process, the pipe was measured to have a 0.786in (0.0200m) wall thickness and an outer radius of 29.838in (0.75789m). The pipe size was chosen for several reasons. The natural frequency of the breathing (i.e. n=0) mode is reduced relative to the bending modes (e.g. n=2,3,4…) when the diameter of the pipe is increased. To increase the potential for measurable scattering between the low order circumferential modes and the breathing mode, a large diameter pipe was desired. A larger diameter pipe section also reduces the relative size of the accelerometer footprint relative to the pipe circumference. Additionally, the larger circumference allows more space for instrumentation, attachment of impedance discontinuities, and the use of an impact hammer to apply the excitation force to the inner circumference of the pipe.

2.1.2 Boundary Conditions

Measured response characteristics presented in this paper are compared to those of an ideal cylindrical shell, with free-free boundary conditions. To minimize the effects of the mounting configuration on the measured scattering characteristics, the shell was supported with its axial dimension vertical by four pressurized rubber air springs,

positioned at the 45°, 135°, 225°, and 315° angular locations. This arrangement was chosen so that there are no added stiffness discontinuities in the measurement plane. The four rubber mounts were inflated with air to approximately 20psi (138kPa). At this pressure, the rigid body response of the shell resonates below 10Hz. As demonstrated in later sections, it was found that the mounting of the shell in this manner may have caused some unintended structural scattering in the control ("clean shell") and other test cases.

2.1.3 Instrumentation

The primary focus of the experiments presented in this paper is on the response of low-order shell modes. The responses of the modes of interest are dominated by the radial component of the shell wall motion. Therefore, an array of radially oriented accelerometers was placed around the circumference of the shell, halfway along the axial length. The accelerometers were equally spaced in increments of 10°, resulting in an array of 36 radially-oriented accelerometers. The test was designed to allow for observation of the scattering behavior between low and high order harmonics. The sensor array chosen may resolve un-aliased response from n_r = -17 to n_r = +18. The number of accelerometers used was limited by the ability to attach test masses between sensors while maintaining a uniform sensor distribution.

Accelerometers were located by first measuring the outer circumference of the shell with a pi tape to an accuracy of 1×10^{-3} in. A section of magnet was then measured and cut to the necessary accelerometer spacing. The accuracy of the sensor placement is estimated to be within ±0.005 in (1.27×10^{-4}m). Table 2-1 lists the test equipment used in

this experiment. A PC was connected to an Agilent Technologies VXI mainframe with E1432 data acquisition boards and a fire wire connection. Accelerometers were powered in ICP mode by the data acquisition boards. The excitation force was generated with an electronic instrumented hammer.

Table 2-1: Test Equipment

Quantity	Manufacturer	Model Number	Description
1	**Dell**		Personal Computer
1	**MTS I-DEAS**	Version 10	Data Acquisition and Analysis Software
1	**Agilent Technologies**	E8408A	Data Acquisition Mainframe
1	**Agilent Technologies**	E8491B	IEEE 1394 (Fire wire) Interface Card
2	**Agilent Technologies**	E1432	16 Channel Data acquisition/ DSP Board
1	**PCB Piezotronics**	086C09	Electronic Instrumented Hammer
36	**PCB Piezotronics**	352C66	Voltage Mode Accelerometers (100 mV/g)
4	**Goodyear**	1B5-500	Super-Cushion Air Spring

2.1.4 Data Acquisition

At each of the 36 angular locations where an accelerometer was located, a corresponding force input location was established on the inner circumference of the shell. Test data was acquired in the frequency domain for impacts at each of the angular locations. The FRFs between the impact force and all accelerometers were acquired by the data acquisition system for 15 impacts at each location. The FRFs from the 15 impacts were averaged by the data acquisition software, yielding 36 averaged FRFs for each impact location. The FRFs were computed with:

$$H_{\theta f,\theta r}(f)=\frac{A_{\theta r}{}^{*}(f)\cdot F_{\theta f}(f)}{F_{\theta f}^{*}(f)\cdot F_{\theta f}(f)}, \tag{2.1}$$

where $H_{\theta f,\theta r}(f)$ is the frequency response function of the acceleration at θ_r due to a force input at θ_f, $A_{\theta r}(f)$ is acceleration spectrum, $F_{\theta f}(f)$ is the force spectrum, and (*) denotes the complex conjugate of a function.

Preliminary data were taken to determine the appropriate acquisition parameters for the test. The shell was found to be very lightly damped. To accommodate the long ring-down time associated with this lightly damped structure, data from each impact was recorded for 2 seconds. This yields a data frequency resolution of 0.5Hz. The maximum frequency was chosen to be 3200Hz. This frequency range was chosen to ensure that the response characteristics of the low order bending modes and the breathing mode were adequately captured. Data acquisition was triggered by a rising slope on the input force signal. A pre-trigger delay was used to ensure that the entire force impulse was captured.

FRF data were acquired and stored in I-DEAS data acquisition software. The data were later exported to MATLAB for post processing, as discussed in the next section.

2.2 Data Processing

Data processing methods were developed to present frequency response data in an intuitive format. The goal in the development of the data processing methods presented in this chapter is to transform the test data from the response of individual transducers to forces at individual force locations into an inference of the response at various spatial harmonics to a force wave at a given spatial harmonic. After applying the data processing methods described in this chapter to the raw test data, data can be viewed as a function of the spatial characteristics of both the input force wave and of the resulting structural response wave.

Shell deflection may be expressed as the summation of type types of series. In the first case, the expansion is in terms of the modes of a clean shell. These modes may be represented by sinusoidal harmonics. These basic modes are acted upon by the addition of discontinuities. When the response of a complex cylindrical structure is expressed in terms of these basic shell modes, several response harmonics may be seen when forced by a single sinusoidal harmonic. Alternatively, the deflection could be expressed in terms of the normal mode shapes of the complex shell. In this case, the effects of the discontinuities are embedded in the mode shapes and are not expressed as simple sine or cosine functions. In this paper, force and response data is analyzed in terms of the first type of expansion. This expansion may be analyzed in terms of standing wave or

traveling wave components of the clean shell response. Although these two methods are mathematically equivalent, analysis of data in both domains allows for a full characterization of the structural response of the shell.

2.2.1 Data Format

FRF data as described in Equation 2.1 were assembled into a three-dimensional matrix in the form:

$$\left[H\left(f,\theta_f,\theta_r\right)\right]=\begin{bmatrix} H_{\theta_1,\theta_1}(f) & H_{\theta_1,\theta_2}(f) & \cdots & H_{\theta_1,\theta_{36}}(f) \\ H_{\theta_2,\theta_1}(f) & H_{\theta_2,\theta_2}(f) & \cdots & H_{\theta_2,\theta_{36}}(f) \\ \vdots & \vdots & \ddots & \vdots \\ H_{\theta_{36},\theta_1}(f) & H_{\theta_{36},\theta_2}(f) & \cdots & H_{\theta_{36},\theta_{36}}(f) \end{bmatrix}, \qquad (2.2)$$

where $[H(f,\theta_f,\theta_r)]$ is the matrix of frequency response functions of the acceleration at θ_r due to a force input at θ_f. The data in this array are a function of frequency, spatial location of the response, and spatial location of the force input. Fourier analysis was applied to the two spatial dimensions of the matrix to yield a data set as a function of frequency, the spatial harmonic of the response, and the spatial harmonic of the force input.

2.2.2 Traveling Wave Transformation

The response of the shell may be expressed as either the sum of a series of propagating waves traveling in opposite directions, or as the sum of a series orthogonal

standing waves. The derivation of the traveling wave domain data processing methods is presented in this section.

The response data expressed in traveling wave form is:

$$A_{\vartheta r}(f) = \sum_{n=0}^{N} [A(f, n_r) \cdot e^{-jn_r\theta_r} + A(f, -n_r) \cdot e^{+jn_r\theta_r}]. \tag{2.3}$$

Equation 2.3 may be expressed in matrix form as:

$$[A(f, \theta_r)] = [A(f, n_r)] \cdot [T_{tw}], \tag{2.4}$$

Where $[A(f,\theta_r)]$ is a matrix of acceleration measurements as a function of response location, $[A(f,n_r)]$ is a matrix of accelerations measurements as a function of the spatial harmonics, and $[T_{tw}]$ is the traveling wave transformation matrix:

$$[T_{tw}] = \begin{bmatrix} e^{-j(N-1)\cdot\theta_1} & e^{-j(N-1)\cdot\theta_2} & \cdots & e^{-j(N-1)\cdot\theta_{36}} \\ e^{-j(N-2)\theta_1} & e^{-j(N-2)\theta_2} & \cdots & e^{-j(N-2)\cdot\theta_{36}} \\ \vdots & \vdots & \ddots & \vdots \\ e^{+j(N-1)\cdot\theta_1} & e^{+j(N-1)\cdot\theta_2} & \cdots & e^{+j(N-1)\cdot\theta_{36}} \\ e^{+jN\cdot\theta_1} & e^{+jN\cdot\theta_2} & \cdots & e^{+jN\cdot\theta_{36}} \end{bmatrix}. \tag{2.5}$$

In this equation, N represents the maximum resolvable spatial harmonic (N=# *sensors/2*). The response of the shell as a function of frequency and traveling wave harmonic may be found by applying the inverse of T_{tw} to both sides of Equation 2.4 as shown:

$$[A(f, n_r)] = [A(f, \theta_r)] \cdot [T_{tw}]^{-1}. \tag{2.6}$$

To obtain the data processing method for transforming test data from the response spatial domain to the response traveling wave domain, it is first noted that the FRF in Equation 2.1 s approximately equivalent to the ratio of the acceleration at sensor θ_r to the force input at θ_f:

$$H_{\theta f,\theta r}(f) \approx \frac{A_{\theta r}(f)}{F_{\theta f}(f)} \tag{2.7}$$

The traveling wave transformation matrix may be applied to the numerator of the transfer function at each force input location to create a matrix of FRFs as a function of response harmonic referenced to each force input location:

$$\left[H\left(f,\theta_f,n_r\right)\right] = \left[H(f,\theta_f,\theta_r)\right]\cdot\left[T_{tw}\right]^{-1}. \tag{2.8}$$

Although the test data was acquired at each force input location individually, the resulting data may be used to infer what the structural response would have been had a traveling wave been used as the excitation force. Using superposition, the response of each traveling wave harmonic to a force wave at a given harmonic may be found by summing the product of the transfer function and the desired force input at each force input location. The response of harmonic n_r to a force input at n_f is expressed as:

$$A_{n_f,n_r}(f) = \frac{1}{2N}\cdot\sum_{i=1}^{2N} H\left(f,\theta_f,n_r\right)\cdot e^{-jn_f\theta_i}, \tag{2.9}$$

where $A_{nf,,nr}(f)$ is the acceleration of harmonic n_r to a force input at harmonic n_f. The response was calculated for one unit of force input at harmonic n_f.

The expression may therefore be rewritten as a transfer function. Equation 2.9 arranged in matrix form, and re-expressed as a transfer function is:

$$\left[H\left(f,n_f,n_r\right)\right]=\frac{\left[T_{tw}\right]}{2N}\cdot\left[H\left(f,\theta_f,n_r\right)\right]. \tag{2.10}$$

This result may be combined with Equation 2.8 to find the final expression for converting the raw test data matrix from spatial coordinates to the traveling wave domain:

$$\left[H\left(f,n_f,n_r\right)\right]=\frac{\left[T_{tw}\right]}{2N}\cdot\left[H\left(f,\theta_f,\theta_r\right)\right]\cdot\left[T_{tw}\right]^{-1}. \tag{2.11}$$

2.2.3 Standing Wave Transformation

In the above derivation, test data was transformed to express the shell response characteristics in terms of traveling wave harmonics. Alternatively, the response of the shell may be expressed as a sum of orthogonal standing wave functions as:

$$A_{\theta_f,\theta_r}\left(f\right)=\sum_{n_r=0}^{N}\left(A_s\left(f,\theta_f,n_r\right)\cdot\sin\left(n_r\theta_r\right)+A_c\left(f,\theta_f,n_r\right)\cdot\cos\left(n_r\theta_r\right)\right), \tag{2.12}$$

where A_s is the sine component of the standing wave response and A_c is the cosine component of the standing wave response.

This equation may be rearranged in matrix form as:

$$\left[A(f,\theta_r)\right] = \left[A_s(f,n_r) \quad A_c(f,n_r)\right]\cdot\left[T_{sw}\right], \tag{2.13}$$

where $[T_{sw}]$ is the standing wave transformation matrix given below:

$$\left[T_{sw}\right] = \begin{bmatrix} \sin\{(N-1)\cdot\theta_1\} & \sin\{(N-1)\cdot\theta_2\} & \cdots & \sin\{(N-1)\cdot\theta_{36}\} \\ \sin\{(N-2)\cdot\theta_1\} & \sin\{(N-2)\cdot\theta_2\} & \cdots & \sin\{(N-2)\cdot\theta_{36}\} \\ \vdots & \vdots & \ddots & \vdots \\ \cos\{(N-1)\cdot\theta_1\} & \cos\{(N-1)\cdot\theta_2\} & \cdots & \cos\{(N-1)\cdot\theta_{36}\} \\ \cos\{(N)\cdot\theta_1\} & \cos\{(N)\cdot\theta_2\} & \cdots & \cos\{(N)\cdot\theta_{36}\} \end{bmatrix}. \tag{2.14}$$

In Equation 2.13 and Equation 2.14 , n_r corresponds to the harmonic number of the response component as before. However, in these equations, there are two components to the response, the sine and cosine component. The values of n_r in this form range from 0 to N. The standing wave transformation matrix may be applied to test data as follows:

$$\begin{bmatrix} H_{s,s}(f,n_f,n_r) & H_{c,s}(f,n_f,n_r) \\ H_{s,c}(f,n_f,n_r) & H_{c,c}(f,n_f,n_r) \end{bmatrix} = \frac{\left[T_{sw}\right]}{2N}\cdot H\left(f,\theta_f,\theta_r\right)\cdot\left[T_{sw}\right]^{-1}. \tag{2.15}$$

The resulting frequency response function matrix is divided into 4 sub matrices. The first index of each sub-matrix corresponds to the standing wave component of the response. The second corresponds to the standing wave component of the force input. For example, $H_{s,c}$ corresponds to the set of FRFs in which the sine component of the response is caused by a cosine component of the force.

2.2.4 Alternative Transformations

In addition to the traveling wave and standing wave transformations presented above, two other data transformations are possible by using the two transformation matrices in

Equation 2.5 and Equation 2.14. The response of the standing wave components due to traveling wave force fields may be computed:

$$\left[H_{s,tw}\left(f,n_f,n_r\right)\quad H_{c,tw}\left(f,n_f,n_r\right)\right]=\frac{\left[T_{tw}\right]}{2N}\cdot H\left(f,\theta_f,\theta_r\right)\cdot\left[T_{sw}\right]^{-1}. \tag{2.16}$$

In this equation, $H_{s,tw}$ represents the set of FRFs in which the sine component of the response harmonic n_r is caused by a traveling wave force at harmonic n_f. In this representation, n_f ranges from $-N+1$ to N, while n_r ranges from 0 to N. Similarly, the traveling wave response due to standing wave force fields may be computed:

$$\begin{bmatrix}H_{tw,s}\left(f,n_f,n_r\right)\\H_{tw,c}\left(f,n_f,n_r\right)\end{bmatrix}=\frac{\left[T_{sw}\right]}{2N}\cdot H\left(f,\theta_f,\theta_r\right)\cdot\left[T_{tw}\right]^{-1}. \tag{2.17}$$

Chapter 3

Experimental Results

3.1 Basic Shell Response Characteristics

All data presented in this paper was acquired using a traditional impact hammer and accelerometers. Basic shell response characteristics such as those found with traditional modal analysis techniques are presented in this section. An understanding of the basic response characteristics such as the modal natural frequencies, damping, and mode shape will help with subsequent analysis of the harmonic scattering characteristics of the shell. The natural frequencies found for the shell are compared to those predicted by basic shell theory. Additionally, the response characteristics of the un-modified shell to traveling wave forces are characterized.

3.1.1 Shell Natural Frequencies and Damping

Figure 3-1 shows the measured frequency response function for frequencies ranging from 0 to 1000 Hz between a force input and acceleration response at 0 degrees. Data presented in this figure shows that clean test data above approximately 70 Hz was acquired. The resonant modes shown in this plot demonstrate large frequency separation, as predicted by analytical models. The amplitude of the FRF at each of the resonance frequencies demonstrates that the structure is lightly damped. The natural frequencies of each of the modes shown were identified by examining a modal indicator function. Since

the magnitude of a frequency response function is dominated by the amplitude of the imaginary component at resonance, an estimate of the natural frequencies of the shell for each test case were found as follows:

$$MIF(\theta_f, f) = \sum_{r=1}^{36} \mathrm{Im}\{H(\theta_f, \theta_r, f)\}^2 . \qquad (3.1)$$

Peaks in this function correspond to the frequencies of the major resonances in the structure. Figure 3-2 shows the use of this modal indicator function for the test case in which the shell was not modified by any impedance discontinuities ("Clean Shell").

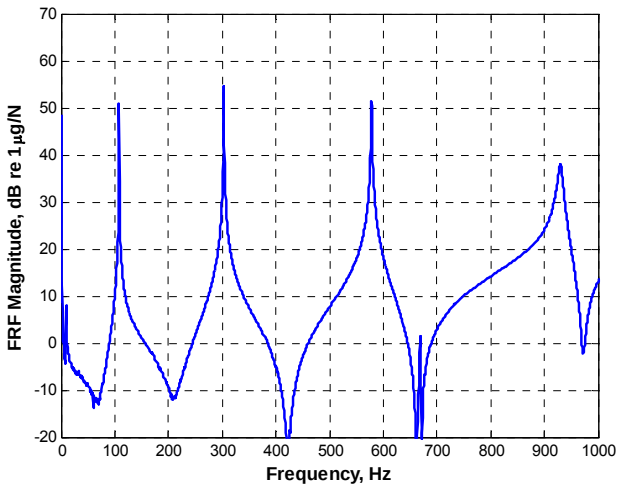

Figure 3-1: Frequency Response Function for Force Input and Acceleration Response at 0 degrees

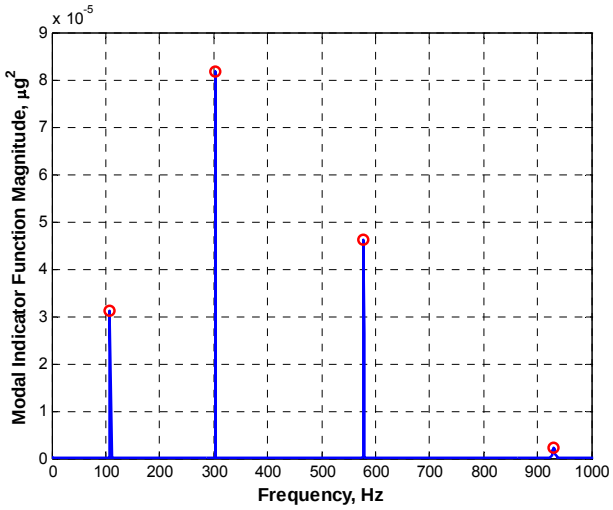

Figure 3-2: Modal Indicator Function for Impact at 0 Degrees to the Clean Shell

Modal analysis was performed on the shell data using I-DEAs software. The polyreference technique was used to identify the major system resonance frequencies and corresponding damping. Table 3-1 lists the results of this analysis. The damping values show that for response harmonics 2, 3, and 4, the structure is lightly damped. The damping in the mode corresponding to a response harmonic of 5 appears to be more damped than the lower order modes. The data was acquired such that a frequency resolution of 0.5 Hz was achievable. Since the structure is lightly damped, the accuracy of the damping values may be limited by the ability to capture the peak of a resonance at the center of a frequency bin.

Table 3-1: Resonance Frequencies, and Damping for Measured Shell Modes

Frequency, Hz	Damping (%)
(n =2) 107.94	**0.035**
(n =3) 303.20	**0.047**
(n =4) 578.20	**0.088**
(n =5) 928.91	**0.428**
1285.67	**0.567**
1362.98	**0.146**
1487.90	**0.157**
1688.02	**0.045**
1860.67	**1.8**
2093.65	**0.227**
2221.41	**0.081**
2338.80	**0.394**
2426.38	**0.059**
2811.24	**0.093**
2829.57	**0.209**

3.1.2 Mode Shapes

Although the data processing methods presented in Chapter 2 will allow for an inference of the harmonic content of the low order, radial dominated modes, the mode shape for the low order modes was observed to ensure data quality. Figure 3-3 shows an estimate of the mode shape for the mode with a resonance frequency occurring at 108 Hz. As expected, the shape of the mode is dominated by a sinusoid with a periodicity of 2. A cosine function was also included in the Figure for comparison. To achieve overlap between the cosine function and the test data, the cosine function had to be spatially shifted. As will be discussed in later sections, this may indicate the presence of a standing wave pattern with a preferred orientation relative to the coordinate system of the shell.

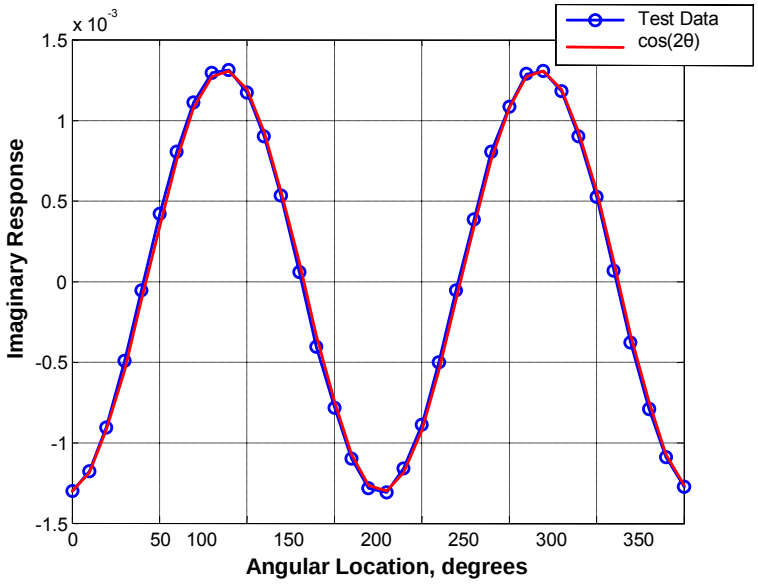

Figure 3-3: Comparison of Spatial Response at n=2 Resonance and a Cosine Function

3.1.3 Direct Traveling Wave Response ($n_f = n_r$)

To better demonstrate the fundamental response characteristics of the clean shell, the data processing methods described in Chapter 2 were applied to the test data. Figure 3-4 shows the FRF magnitude of the direct traveling wave terms for the shell without added mass discontinuities. Direct terms are defined as the response of a traveling wave at a given harmonic to a force input at the same harmonic (i.e. $n_f = n_r$). In this figure, it is seen that the modal density of the structure increases significantly above 1000 Hz. The harmonic components shown in Figure 3-4 demonstrate a "clean" response as a function of frequency. This shows that the data processing methodology was successful in filtering both the force and response dimensions of the test data into its

spatial components. The responses of the $n_r = 4$ and 5 modes appear to increase at a rate of 40 dB per decade at frequencies below the first resonance. This is consistent with the expected behavior of a single degree of freedom system in the stiffness dominated region of its response. The responses of lower order modes do not demonstrate this same trend. Difficulties in acquiring low frequency data due to the lightly damped nature of the structure may have yielded non-physical response data at low frequencies for these modes. Additionally, scattered energy from the rigid body responses below 10 Hz may contribute to the deviation from expected response at low frequencies.

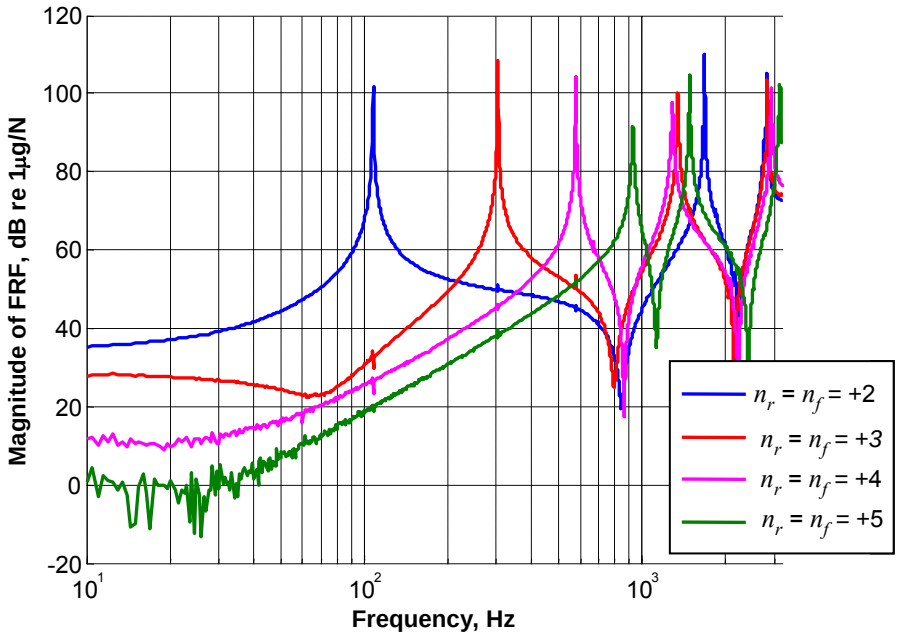

Figure 3-4: Direct Traveling Wave Response FRFs for Excitation and Response Harmonics 2 through 5

3.1.4 Comparison to an Analytical Model

A simple analytical model of the direct term response was created for comparison to test data. The natural frequencies of shell modes with uniform axial distribution were predicted by inextensional vibration theory in Reference [1], according to the equation:

$$\omega_{n,0} = \frac{n \cdot \left(n^2 - 1\right)}{\left(n^2 + 1\right)^{1/2} \cdot a} \cdot \left(\frac{h^2}{12a^2}\right)^{1/2} \cdot \left[\frac{E}{\mu \cdot \left(1 - \nu^2\right)}\right]^{1/2}, \tag{3.2}$$

where $\omega_{n,0}$ is the natural frequency of a mode with a circumferential harmonic n and no axial variation. For the purposes of this analysis, it was assumed that the shell had free-free boundary conditions. The natural frequencies for modes with non-uniform axial distribution (ω_{mn}) were predicted using the general solution presented in Reference [1]. Figure 3-5 compares the measured natural frequencies to those predicted by the analytical model. In general, the characteristics of the predicted and measured frequencies are in good agreement.

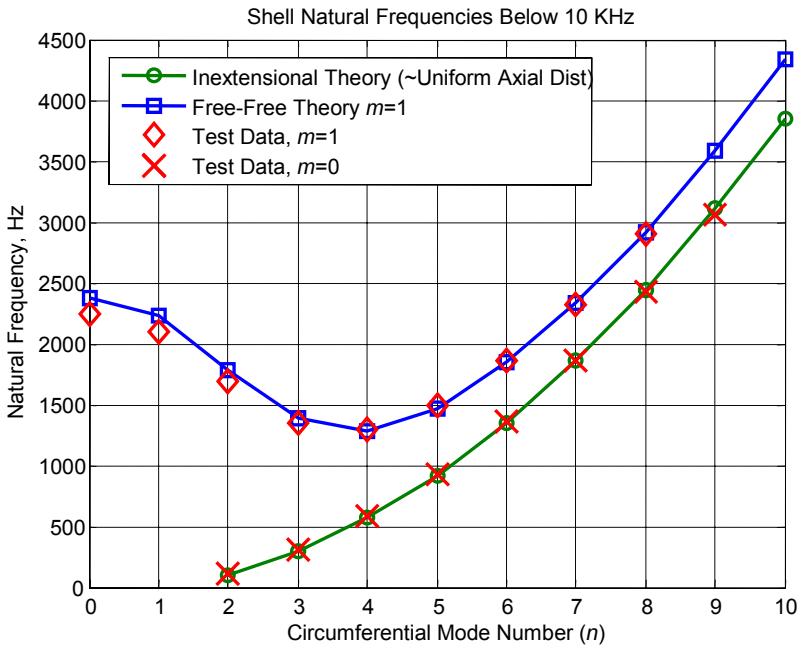

Figure 3-5: Comparison of Measured and Predicted Natural Frequencies

3.1.5 Scattering Characteristics in the Clean Shell

In an ideal cylinder, the response to a force at a given harmonic contains harmonic content only at the harmonic equal to that of the force. Although attempts were made to minimize the scattering in the clean shell, measured response characteristics appear to deviate from that expected of an ideal cylinder. In order to understand the effect of adding impedance discontinuities on the scattering characteristics, the scattering characteristics of the unmodified shell must first be analyzed. Figure 3-6 shows the positive and negative traveling wave components of response harmonics 1 through 5 to a force at $n_f = +2$. As expected, the response is dominated over the majority of the frequency range by the direct term, $n_r = +2$. Over the majority of the frequency range,

the scattered response ($n_r \neq +2$) is at least 30dB lower than the direct response. However, at the resonance frequency of each of the harmonics shown, the response of that harmonic is greater than the direct response. Additionally, it is noted that the response of the $n_r = -2$ harmonic is nearly equal in amplitude to the positive traveling direct term. This indicates that the response of the shell at the resonance frequency is dominated by a standing wave response. At frequencies away from the resonance frequency, the response of the negative traveling wave is less than the direct term, indicating that a traveling wave dominates the response.

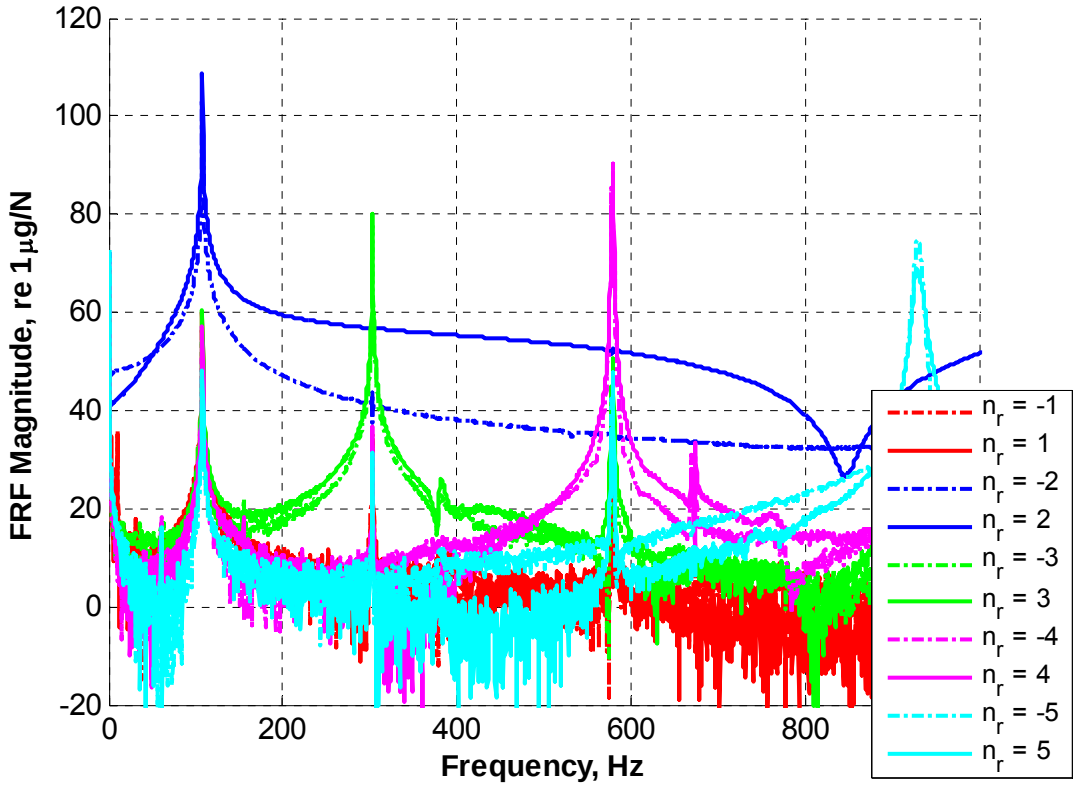

Figure 3-6: Primary and Scattered Response Amplitudes for a Force Input at $n_f = +2$

Figure 3-7 is a three dimensional plot showing the magnitude of the FRFs for all response harmonics from -15 to +15 to a force input at n_f = +2. In this type of plot, the ideal cylinder response would appear as a single line at n_r = +2 across the frequency range. Responses at other harmonics would not be present. A threshold of 20dB was used to generate the plot in Figure 3-7 so that only responses above the noise floor are shown. The white squares correspond to the response of scattered harmonics at their resonance frequencies.

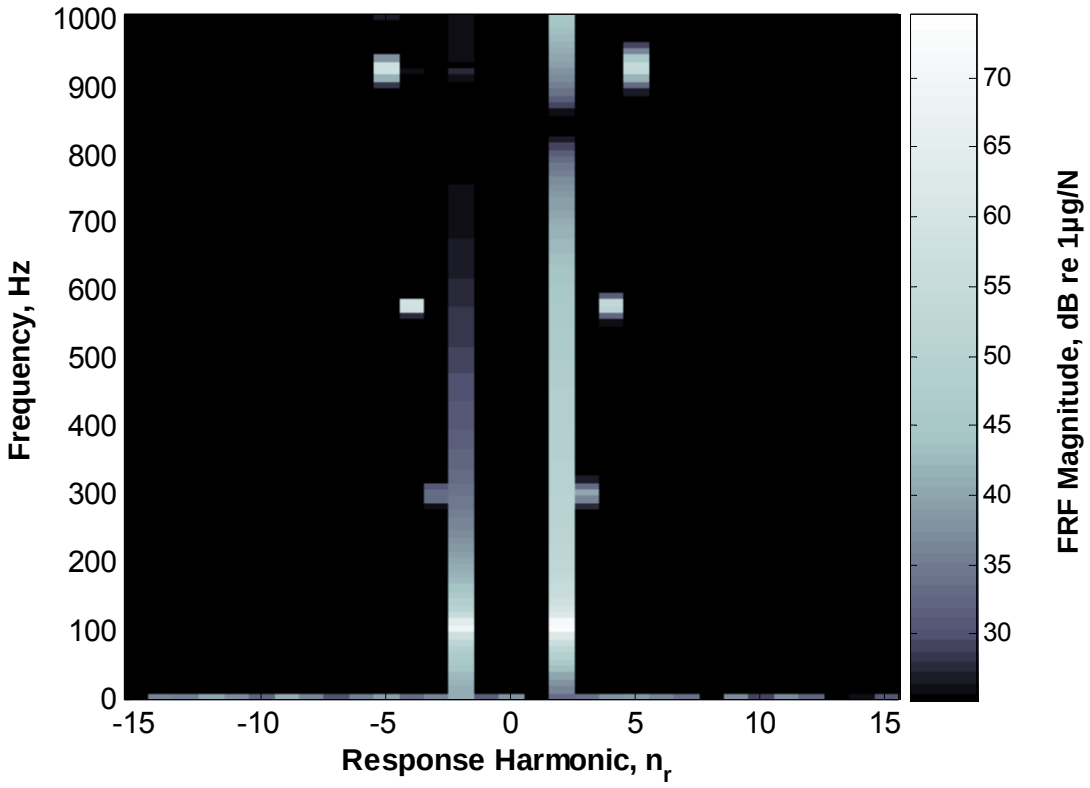

Figure 3-7: Frequency Response Magnitude of the Clean Shell for a Force Input at n_f = +2

The unexpected response characteristics suggest that there are characteristics of the clean shell that cause energy to be scattered from the primary forcing harmonic into

other harmonics. Two potential characteristics of the clean shell that may yield structural scattering are the weld seam and the boundary conditions. Evidence confirming these as potential scattering mechanisms will be discussed in later sections, after demonstrating the effects of added impedance on the scattering characteristics. In addition to the physical characteristics of the clean shell that may yield scattering, inaccuracies in the measurement process could also increase the scattering present in the clean shell case. Errors in the accelerometer calibrations (amplitude and phase) could increase the amount of apparent scattering. Additionally, variation in the spacing of either accelerometers or force impacts could increase the measured level of scattering.

3.2 The Effect of Periodically Attached Masses

To assess the effect of attaching masses periodically to the cylindrical structure, 3 masses were attached around the outer circumference of the shell at the 55°, 175°, and 295° locations (120° apart). The total weight of each of the masses was 17.6±0.2lbs (7.7±0.09kg). The masses were attached as shown in Figure 3-8 and Figure 3-9 with loctite glue and nylon straps. Each of the attached masses consisted of two parts. The first was a 5.5lb (2.5kg) steel block. As shown in Figure 3-8, this steel block was oriented such that a minimal percentage of the circumference of the shell was occupied by the footprint of the attached structure. By attaching the structure in this manner, the added impedance in the circumferential direction is expected to be dominated by the mass of the attached structure. However a consequence of this attachment method is that the attached structure may increase the stiffness of the shell in the axial direction. Data presented in

this section demonstrates the effect of adding periodically attached masses to the structure. The sensitivity of these scattering characteristics to a change in the mass of the attached structure is also demonstrated.

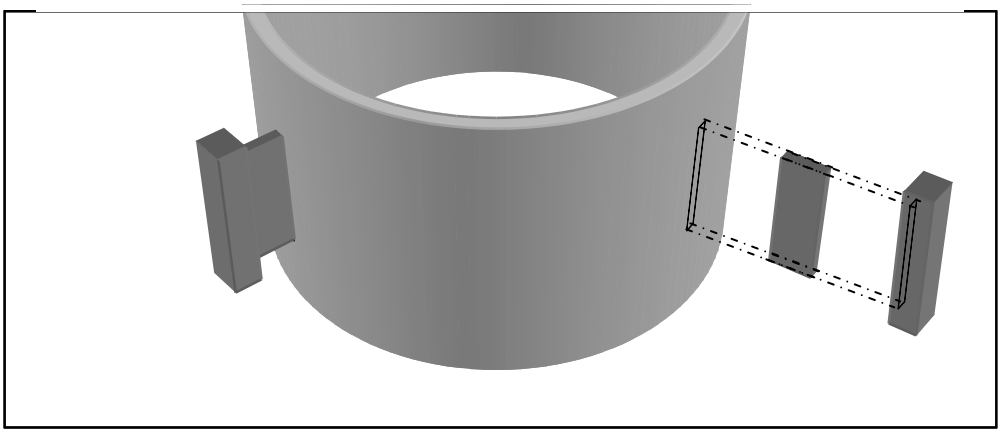

Figure 3-8: Diagram Demonstrating the Attachment of Masses to the Shell

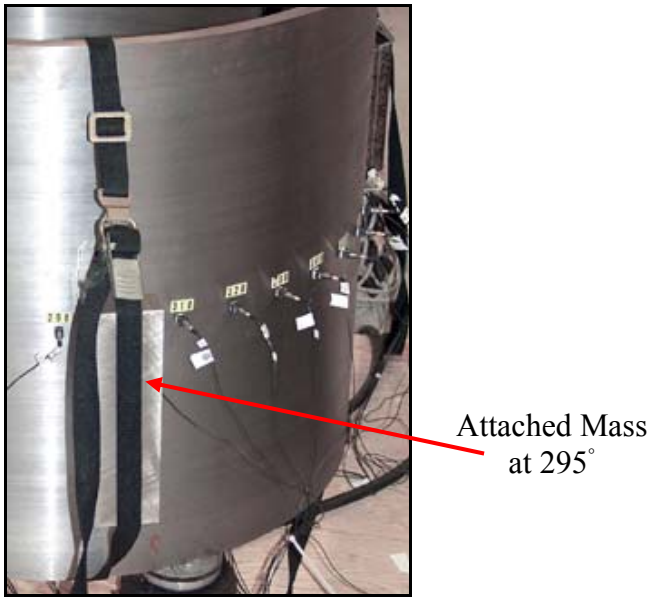

Figure 3-9: Picture of one Mass Attached to the Shell

3.2.1 Direct Response Characteristics

The response of an ideal shell may be characterized by two orthogonal modes at the same frequency. These modes have no preferred orientation relative to the angular coordinate of the shell. The response of these modes will be positioned with the same orientation as the input force wave. Therefore, the response of an ideal shell to a traveling wave is a traveling wave of the same harmonic. When periodic masses were added to the structure, it was found that the mode at the response harmonic equal to the number of attached masses was split into two distinct modes at different frequencies. Figure 3-10 compares the direct response of the n_r = +3 mode for the test case in which no masses were attached and for the case in which 3 periodic masses were attached. This figure demonstrates the mode-splitting effect that the addition of periodic massed has on the mode at the harmonic equal to the number of masses. Prior to adding masses, the first *n=3* bending mode occurred at 303Hz. After adding the three 17.6lb (7.7kg) masses, two *n=3* bending modes are seen at 306Hz and 279.5Hz. The distance between the resonance frequencies of the split mode appears to be related to the amount of mass added to the structure. Assuming constant modal stiffness, the square of the ratio of the frequencies is inversely proportional to the ratio of the modal masses:

$$\left(\frac{f_1}{f_2}\right)^2 = \frac{k_1 / m_1}{k_2 / m_2} = \frac{m_2}{m_1}, \tag{3.3}$$

where f_1 and f_2 are the resonance frequencies before and after the addition of masses, k_1 and k_2 represent modal stiffness before and after the addition of mass, and m_1 and m_2 represent the modal mass before and after the addition of masses. The estimated mass

ratio (m_2/m_1) is 1.24, while the square of the frequency ratio is approximately 1.20. A similar phenomena may be present for other integer multiples of the number of masses (e.g. $n_r = 6, 9,\ldots$) however, the effect was difficult to measure since the cut-on frequency of these modes occurs above the cut-on frequency of some m=1 modes, yielding a high modal density in the frequency region of the resonances.

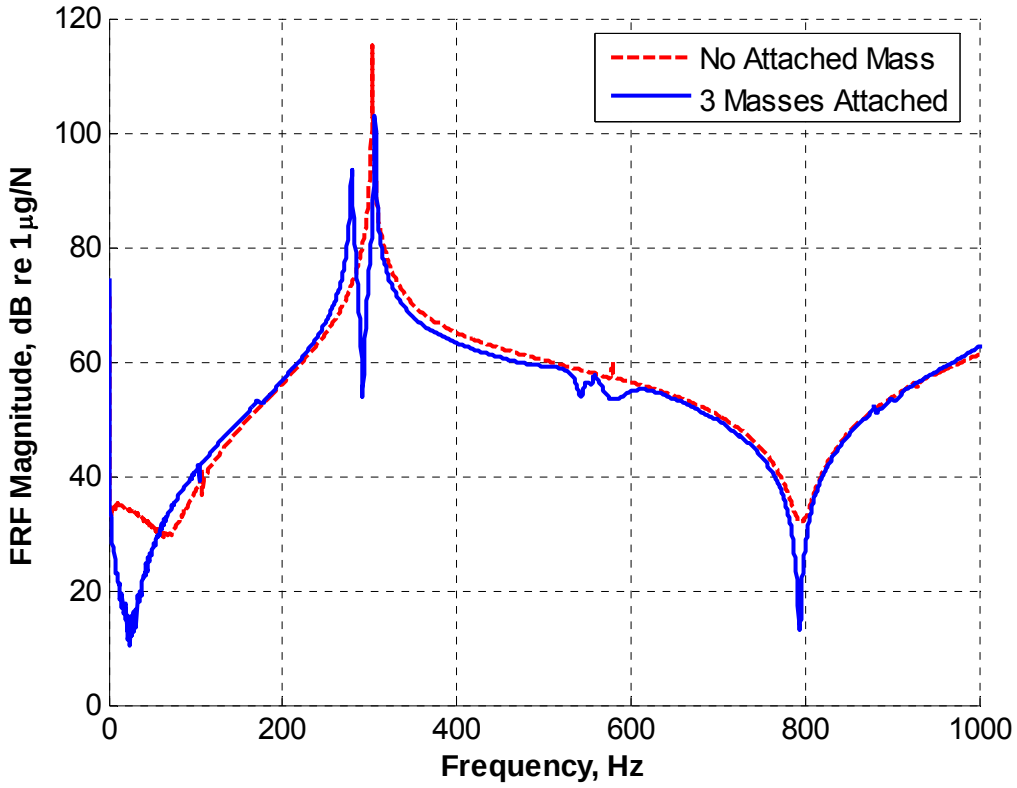

Figure 3-10: Traveling Wave Frequency Response of the n_r = +3 Harmonic to a Force at n_f = +3 for the Clean Shell and 3 Periodic Mass Test Cases

The test data suggests that when periodic masses are attached to the structure, the mode splitting occurs at the response harmonic equal to the number of masses because the masses participate in the motion of one of the two modes, while they are located at the nodes of the other mode. Therefore, the modal mass of the two modes at that

response harmonic are different. This behavior occurs when the response modes take on a preferred orientation relative to the angular coordinate system of the shell. The tendency of the mode to take preferred orientations is demonstrated in Figure 3-11. In this figure, the same data used to generate Figure 3-10 was used. However, the sine and cosine components of the response were inferred for a traveling wave at $n_r = +3$. The standing wave transformation applied to the response dimension of the data was rotated until two distinct modes were observed. This occurred at an orientation of 5 degrees. As seen in Figure 3-11, each of the two resonance frequencies of the split mode appear to be due to two standing wave modes at slightly different frequencies. The single degree of freedom nature of each of these curves suggests that the two peaks are due to two separate modes.

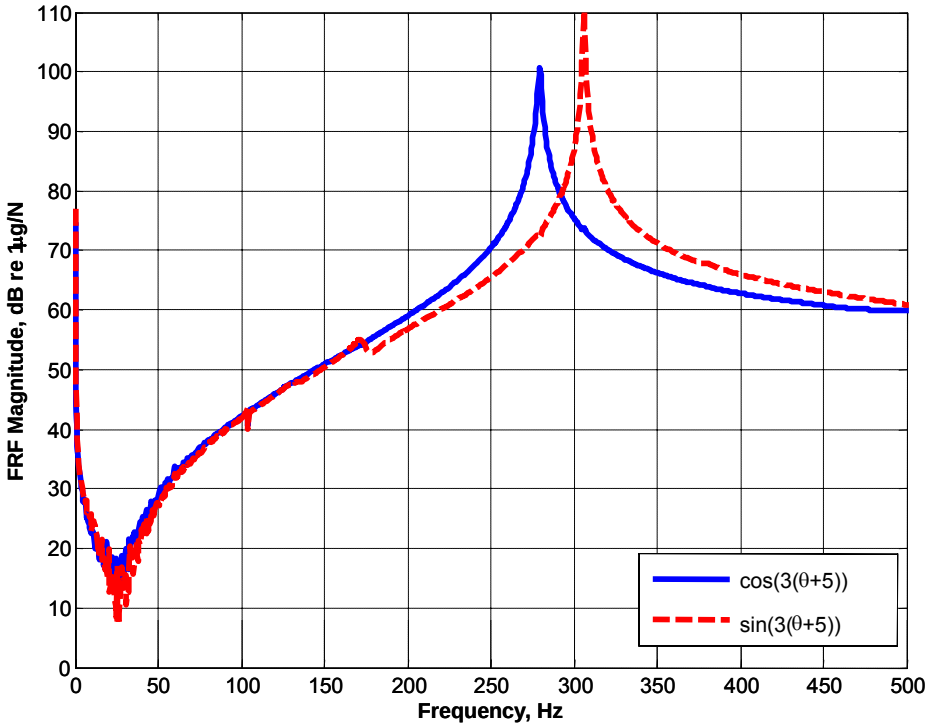

Figure 3-11: Standing Wave Frequency Response of the n_r = 3 Harmonic to a Force at n_f = +3 for the Clean Shell and 3 Periodic Mass Test Cases

Figure 3-12 shows the orientation of the sine and cosine standing wave shapes relative to the shell angular coordinate system. Also shown in the figure are lines corresponding to the locations where the masses were attached. The two modes appear to align such that the masses are at the anti-nodes of the cosine node, while the masses are at a node of the sine mode. This demonstrates that the addition of the masses influences the mode at the same harmonic in two ways. First, the mode is split into two distinct modes. Second, these two modes have a preferred orientation relative to the orientation of the masses. This is consistent with data presented in Figure 3-11 since the low frequency mode, the cosine mode, is the mode in which the masses participate in the response of the

mode. The additional mass due to the attached masses causes the frequency of the cosine mode to decrease relative to that of the sine mode.

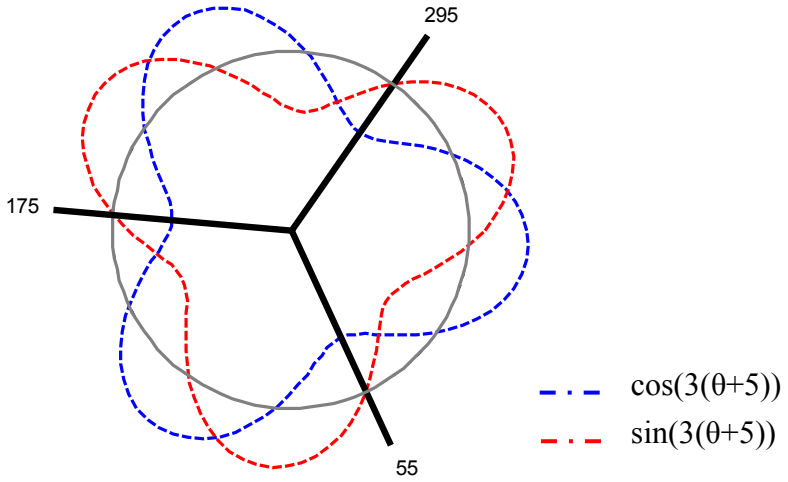

Figure 3-12: Orientations of the sine and cosine Mode Shapes for $n_r = 3$

The unique characteristics of the direct response due to the addition of periodic discontinuities may be used as an indicator of the presence of periodic discontinuities in test data measured from cylindrical structures. Figure 3-13 shows the direct (i.e. $n_r = n_f$) and the backscattered (i.e. $n_r = -n_f$) responses for harmonics 2 through 5 for the clean shell. As seen in this figure, the backscattered response appears to increase at the resonance frequencies. This behavior may be caused by the presence of a weld seam. Since the seam has a periodicity of 1, all harmonics could be affected. However, the difference between the direct and backscattered responses at $n_r = 4$ is much lower than for the other modes shown. This may indicate the presence of another physical characteristic in the clean shell that causes scattering. Figure 3-14 and Figure 3-15 show the response of the $n_r = \pm 4$ harmonics to a force wave at $n_f = +4$ for the clean shell test case. At frequencies away from the resonance frequency, the response is dominated by a

traveling wave at the same harmonic as the force input wave. However, the response of the negative traveling wave is nearly equal to the positive traveling wave at the resonance frequency. Figure 3-15 also shows that the $n_r = 4$ mode is split into two separate resonance frequencies. The similarity between the direct response characteristics of the clean shell to a $n_f = +4$ force and the shell with three periodically attached masses to a $n_f = +3$ force suggests that a periodic impedance with a multiplicity of 4 may be present in the clean shell. The most likely cause of these characteristics is the presence of the four mounts, which may add some stiffness in the radial direction at on end of the shell.

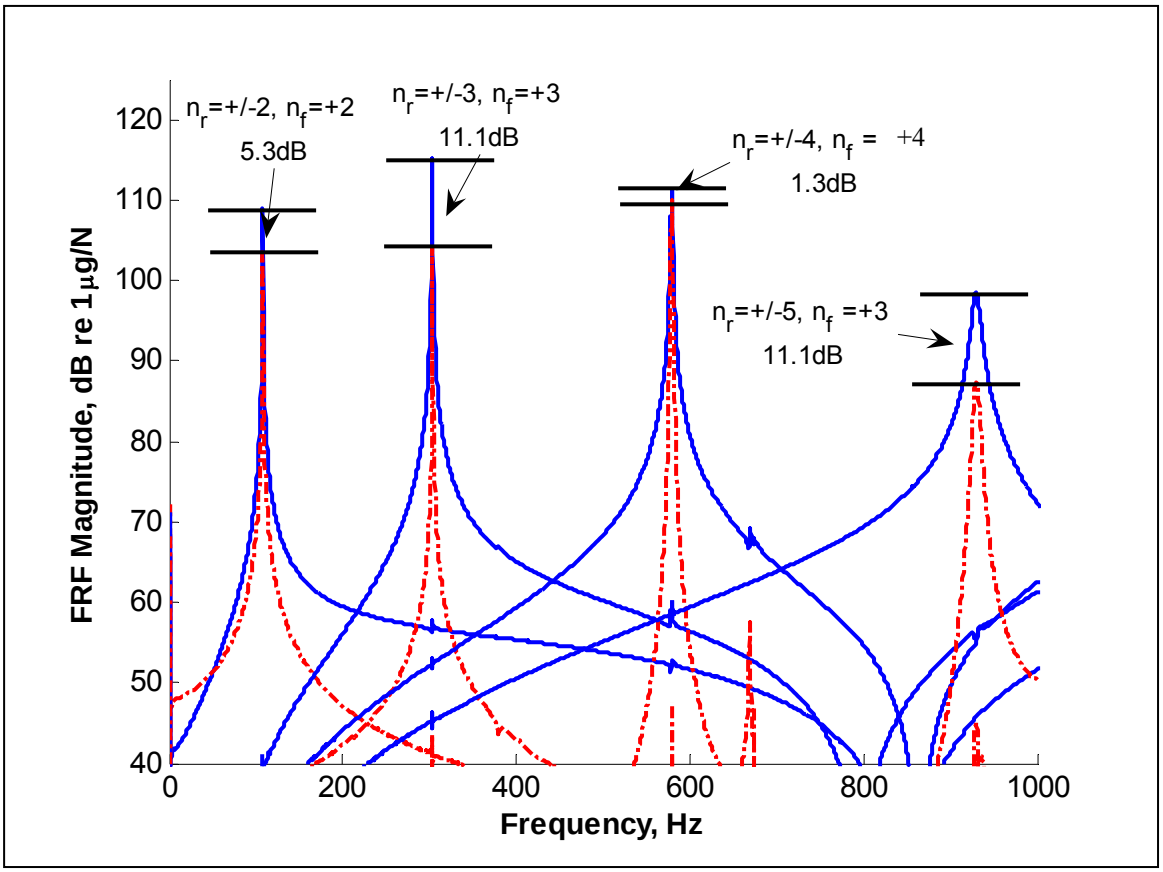

Figure 3-13: Direct (i.e. $n_r = n_f$) and Backscattered (i.e. $n_r = -n_f$) Responses for Harmonics +2 through +5

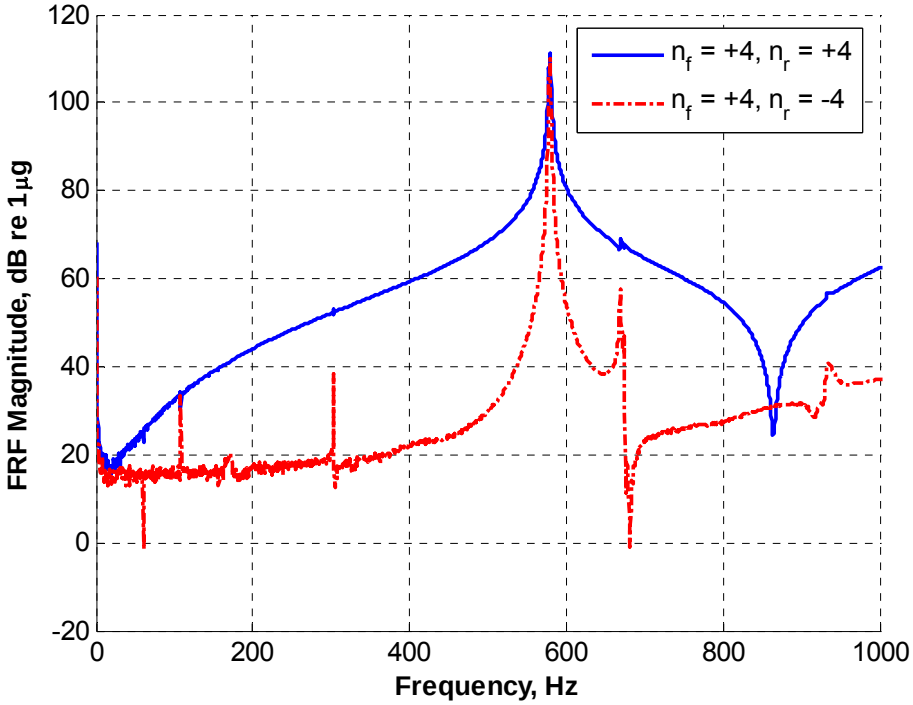

Figure 3-14: Traveling Wave Frequency Response of the n_r = ±4 Harmonics to a Force at n_f = +4 for the Clean Shell

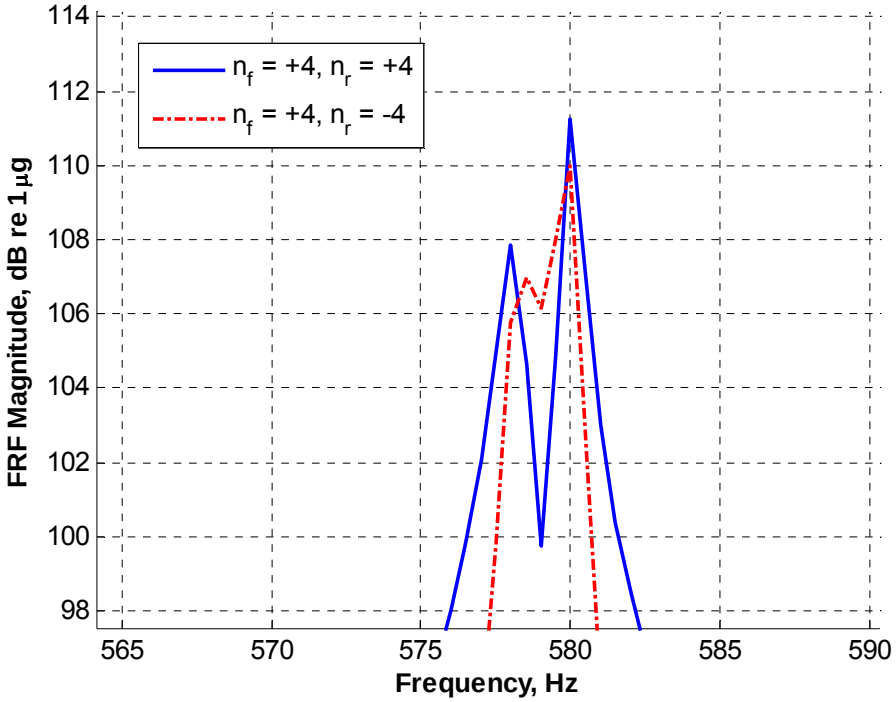

Figure 3-15: Traveling Wave Characteristics at the n = 4 Resonance Frequency to a Force at n_f = +4 for the Clean Shell

3.2.2 Scattering Characteristics

As shown in Chapter 4, some degree of structural scattering existed in the in clean shell prior to the attachment of the masses. Data for cases in which masses were added contains scattering due to both the scattering characteristics of the clean shell and the characteristics due to the addition of the masses. Data for the attached mass cases are therefore compared to data for the clean shell case to infer the changes caused by the addition of the masses. The most notable effect of adding masses to the shell is demonstrated in Figure 3-16. In this figure, the response to a traveling force wave a n_f =

+2 was averaged over the entire data acquisition frequency range (0-3200Hz). Although the response in most harmonic appeared to increase when the periodic masses were attached, there was a significantly greater increase in response for harmonics that are related to the number of attached masses and the forcing harmonic according to the relationship:

$$n_r = n_f \pm kZ, \quad where\ k = 1,2,3,... \tag{3.4}$$

This result is consistent with the FEA analysis presented in Reference [2].

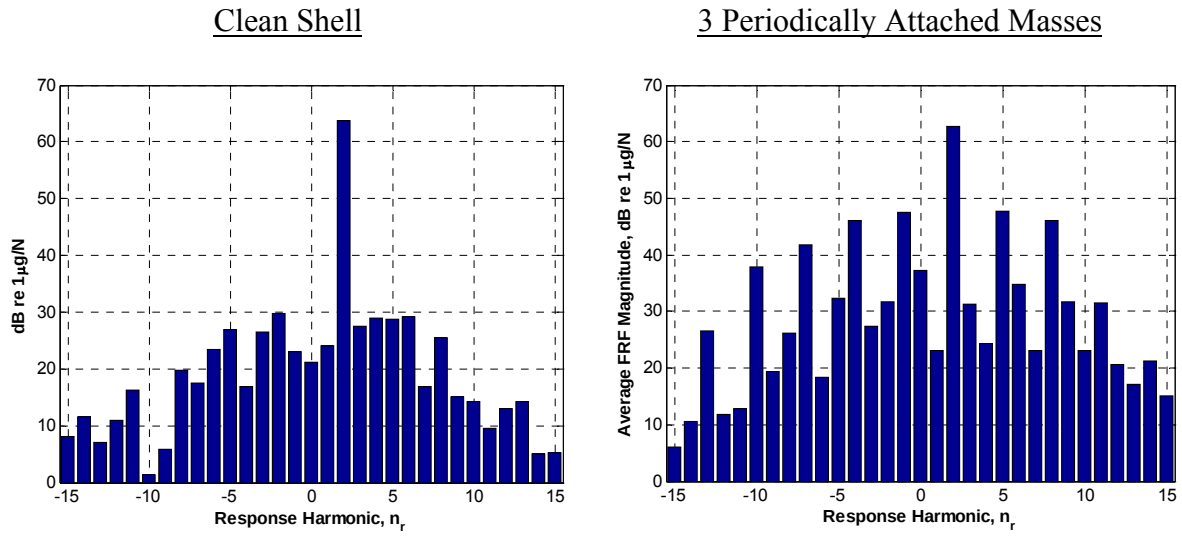

Figure 3-16: Comparison of the Average Frequency Response Magnitude (0-3200 Hz) Between the Clean Shell and Periodic Mass Test Cases

Although Figure 3-16 provides a good view of the overall trend in the data when masses are added, unique characteristics in the response may be missed if the frequency dependant nature of the scattering effects is not analyzed. Figure 3-17 shows the response of the positive and negative traveling wave components to a force at $n_f = +2$ for the first 5 harmonics. When compared to Figure 3-6, it is seen that the response of the

indirect terms (scattered response) appears to increase for all harmonics across the frequency range. However greater increase in response is observed in harmonics that follow the relationship in Equation 3.4. The response of the shell for all harmonics from -15 to 15 to the same traveling force wave at $n_f = +2$ are shown in Figure 3-18.

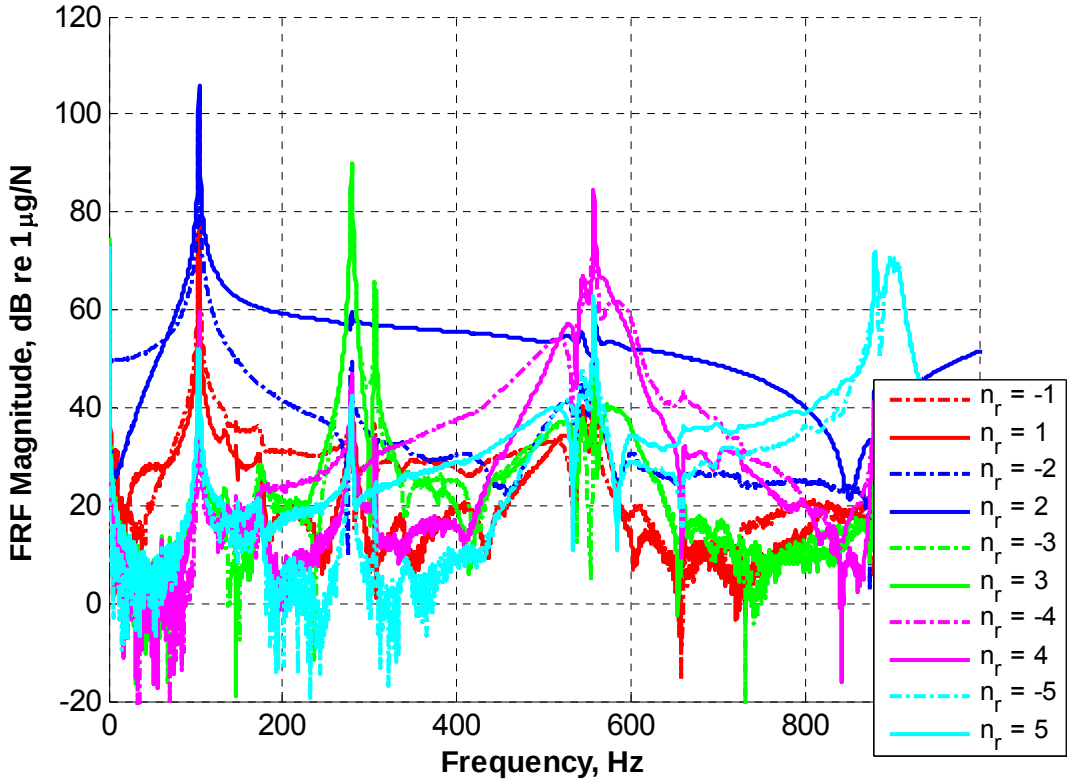

Figure 3-17: Frequency Response Spectra from $n_r = \pm 1$ through ± 5 Due to a Force Input at $n_f = +2$ for the 3 Periodic Mass Test Case

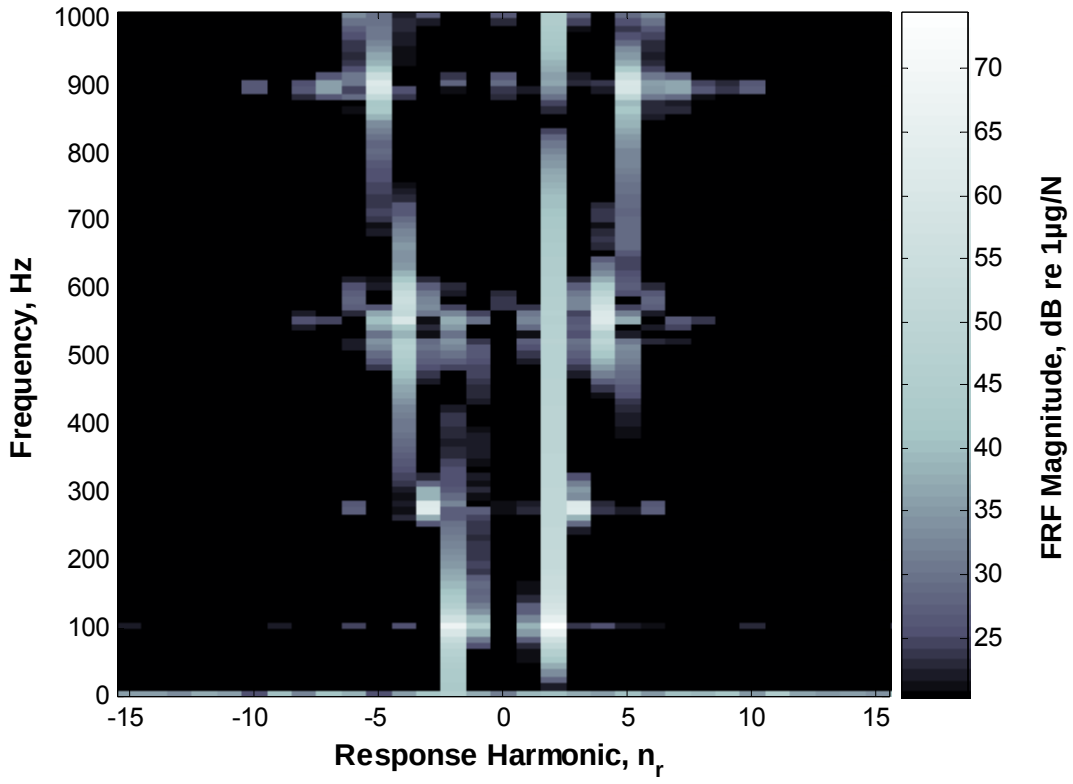

Figure 3-18: Frequency Response Magnitude Due to a Force at $n_f = +2$ for the 3 Periodic Mass Test Case

When the spatial harmonic of the forcing function is equal to the number of periodically attached structure, energy is scattered into the radial breathing mode (i.e. $n_r = 0$). Figure 3-19 shows the change in the scattered response of the breathing mode to a forcing function at $n_r = +3$ when 3 periodic masses are added to the structure. In this figure, it is shown that the response of the breathing mode appears to increase across the entire frequency range. Below the resonance frequency of the $n = 3$ mode, significant change was not measured.

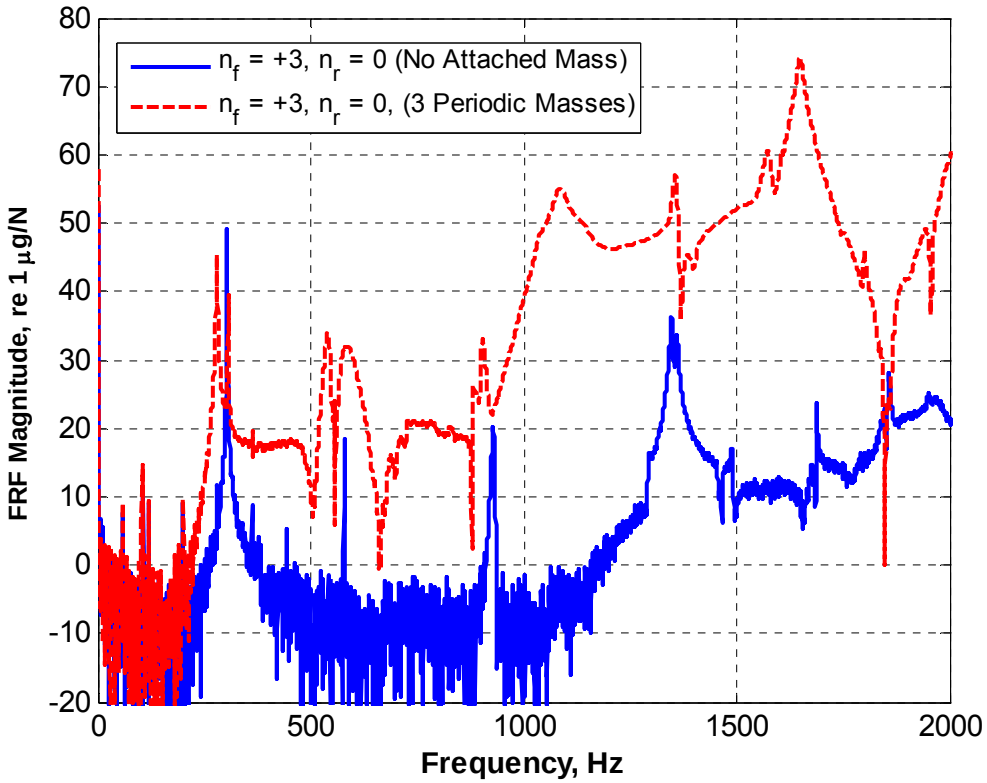

Figure 3-19: Change in Response of the Breathing Mode (n_r = 0) to a Force at n_f = +3 When 3 Periodic Masses are Attached

3.2.3 Change in Scattering Characteristics

It is difficult to infer scattering characteristics unique to the addition of the periodic masses in Figures3-17 and 3-18. To better demonstrate the change in scattering characteristics due to the addition of the periodic masses, the change in scattering from the clean shell test case is computed as:

$$\Delta S(n_r, n_f, f) = S_1(f) - S_2(f) \tag{3.5}$$

where $S_1(f)$ and $S_2(f)$ represent the scattering from the direct to indirect terms for the clean shell and shell with masses, respectively. The value of S_1 is computed as:

$$S_1 = 20 \cdot \log_{10}\left(\frac{H_1(n_f, n_f, f)}{dB_{ref}}\right) - 20 \cdot \log_{10}\left(\frac{H_2(n_f, n_r, f)}{dB_{ref}}\right). \quad (3.6)$$

Figure 3-20 demonstrates the values of S_1 and S_2 graphically.

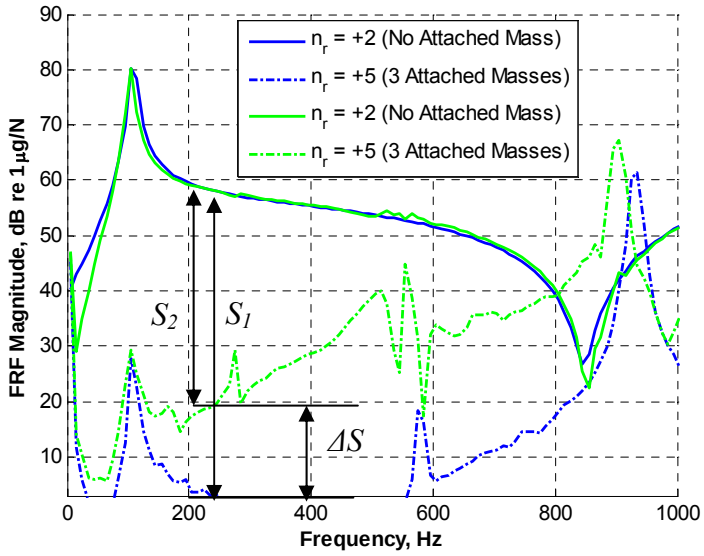

Figure 3-20: Demonstration of the Computation of the Change in Scattering

Figure 3-21 plots the change in scattering between the clean shell and the shell with three periodic masses for a force input at $n_f = +2$. The vertical yellow lines in this figure indicate the response harmonics where increased scattering is expected due to the added masses. The effect of adding the masses on the scattering characteristics of the shell may be more clearly seen in this figure than in Figure 3-18. Across the frequency range, the most significant change in scattering is found at the expected response harmonics. Increases at unexpected harmonics appear to occur at the low order shell mode resonance frequencies. This may be an artifact of the noise floor on the data. In

reality, scattering into all modes is likely present to some level due to variability in instrumentation placement, instrumentation sensitivities, mass placement, etc. The scattered response in these modes may be immeasurable except at the resonance frequencies where the scattered response is increased above the level of the noise floor.

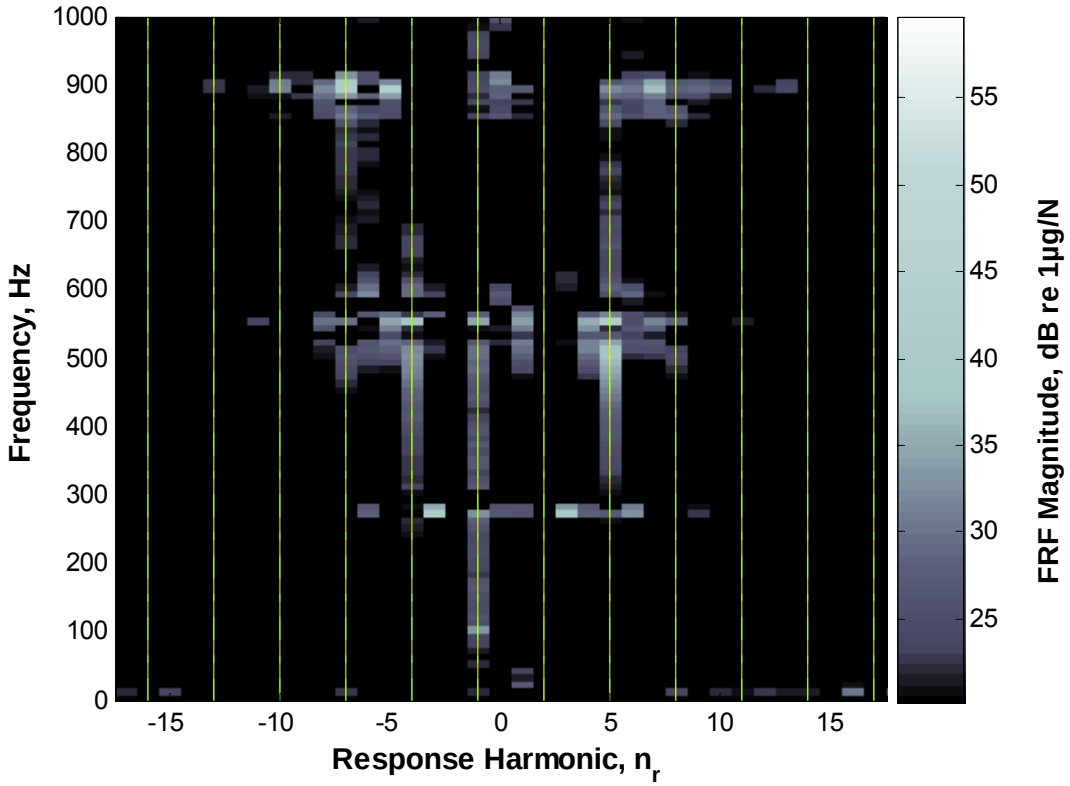

Figure 3-21: Change in Scattering from the Clean Shell to the Shell with 3 Periodically Attached Masses with a Force Input at n_f = +2

Figure 3-21 shows that the greatest change in scattered response appears to occur in the modes with the highest mobility. This also may be a limitation due to the noise floor in the data. Higher order modes may still respond in the frequency range presented. Figure 3-22 shows the change in scattering for a force at n_f = -4. As shown for the n_f =

+2 case, the greatest change in scattering characteristics is seen at response harmonics separated by the number of masses added, consistent with Equation 3.4.

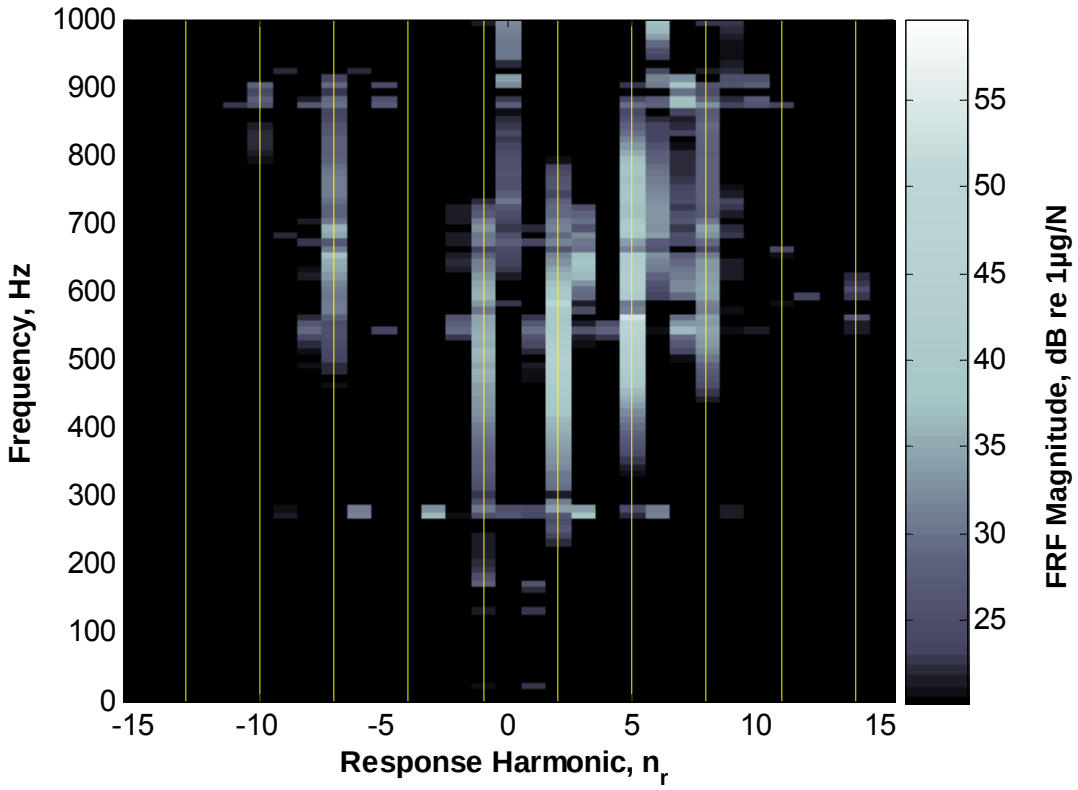

Figure 3-22: Change in Scattering from the Clean Shell to the Shell with 3 Periodically Attached Masses with a Force Input at n_f = -4

3.2.4 Frequency Dependent Characteristics

Depending on the type of impedance discontinuity attached to the structure, the spectral shape of the response may vary. Figure 3-23 shows the scattered response of the dominant response harmonics found in Figure 3-21. At frequencies where a response was measured above the noise floor, the scattered response appeared to follow a

40*$\log_{10}(f)$ trend until peaking at a resonance frequency. This trend is similar to that of the response of a mode in a stiffness dominated region. This indicates that there is little frequency dependency of the energy scattered into each of the harmonics. In other words, the scattered response of each harmonic appears to have a shape similar to the mode at that harmonic. If the energy scattered into the mode was not constant with frequency, the scattered response may take on a different shape.

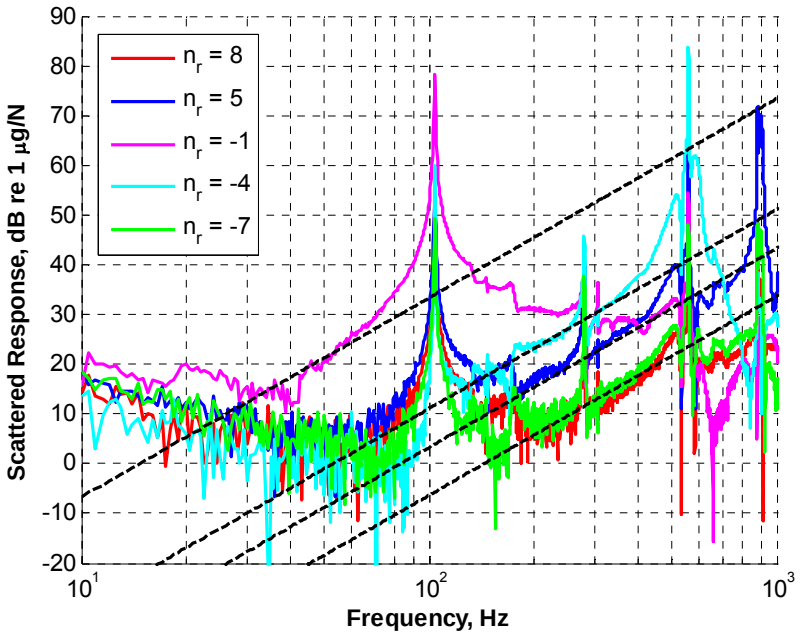

Figure 3-23: Dominant Scattered Response Harmonics for a Force input at $n_f = +2$

The responses of the structure at harmonics other than those that follow Equation 3.4 do not appear to exhibit the same frequency dependent trend. Instead, the scattered response appears to increase rapidly near resonance frequencies. This behavior is shown in Figure 3-24, where the changes in scattered response for harmonics -8 through +8 are shown. The dominant harmonics previously shown in Figure 3-23 are shown in color, while responses at other harmonics are shown in grey. The scattered

response at these harmonics appears to increase at a greater slope than the dominant harmonics.

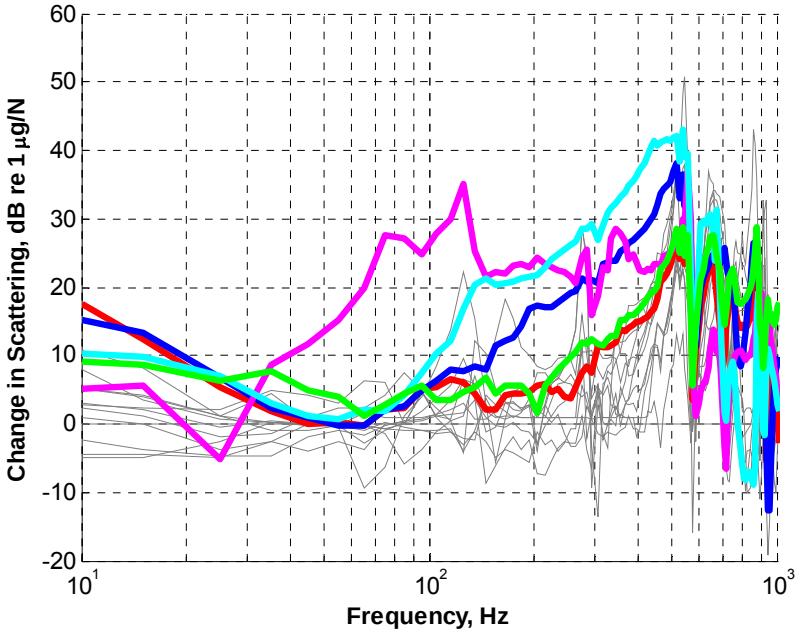

Figure 3-24: Change in Scattering from the Clean Shell to the Shell with 3 Periodically Attached Masses with a Force Input at n_f = +2

3.2.5 Sensitivity to Mass of Attached Structure

A test was conducted in which the each of the periodically attached masses was 5.5 lbs, rather than the 17.7 lbs presented in the majority of this paper. Figure 3-25 shows a comparison of the frequency responses of the n_r = +2 harmonic for an input force applied at the n_f = -4 for the test cases with the two different masses. The data shown in this figure demonstrates that as the mass of the attached structure is increased, the amount of energy scattered into the indirect response harmonics increases. This sensitivity to

mass only appears to occur at frequencies below approximately 1000 Hz. Above this frequency, any differences in the two plots appear to be due to the shift in natural frequency of the response modes due to the increased impedance. The reason for the lack of change in scattered energy at the higher frequencies may be explained by the inability to attach structure whose impedance is dominated by its mass. Based on the orientation of the attached structure, it is likely that significantly more stiffness was added along the axial dimension than in the circumferential. The modes above 1000 Hz are predicted to have higher order axial content, while the modes below 1000 Hz are predicted to have a uniform axial response ($m = 0$). The scattering characteristics at higher frequencies may therefore be dominated by the added axial stiffness than by the mass. Since the footprint of the attached structure did not change with added mass, the stiffness of the attached structure may not have changed significantly between the two test cases.

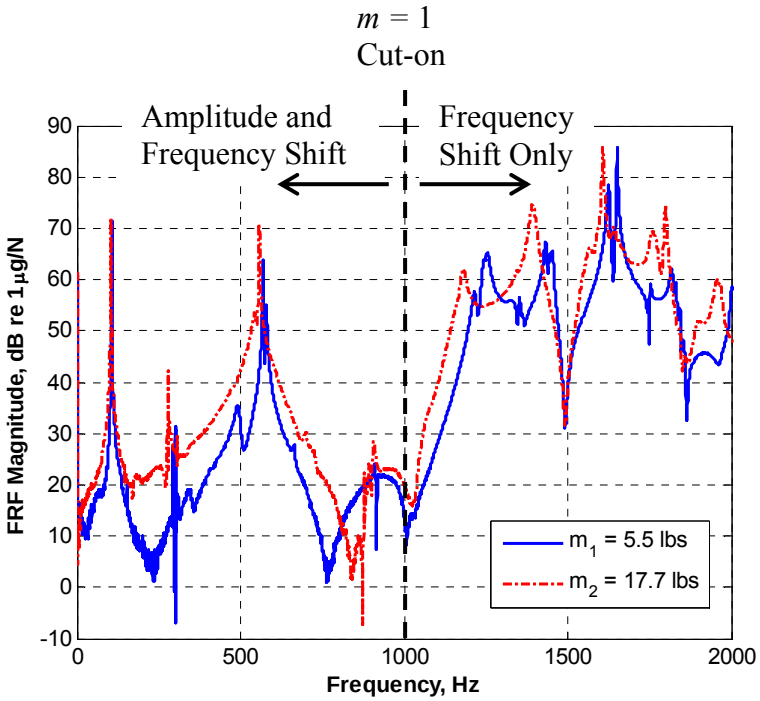

Figure 3-25: Frequency Response of the n_r = +2 Harmonic Due to a Force at n_f = -4 for Two Different Periodic Structure Masses

Figure 3-26 compares the transfer functions of the two attached mass cases for a response at the n_r = +5 harmonic to a force input at the n_f = +2 harmonic. Similar trends in the data are seen. Below approximately 1000 Hz, the amount of scattered energy increases with increased attached mass. Above 1000 Hz, the amount of scattered energy appears to change only due to the change in modal frequency with the addition of more mass. Comparison of the two Figures also reveals that the amplitude of the response at the resonance frequency of the n_r = 3 and n_r = 4 modes increases with added mass. However, the scattered response at the n_r = 2 and n_r = 5 modes does not appear to change significantly. The lack of change in scattered response at these frequencies may indicated that the scattering characteristics are dominated by other characteristics of the system than the periodically attached masses. Due to the shift in resonance frequencies and

variability in test data, an exact measure of the change in scattering due to the mass increase was not measured. Additionally, only two data points were obtained. However, it is observed that the scattered energy at the expected harmonics increases between 5 and 10 dB when 12.2 lbs. are added.

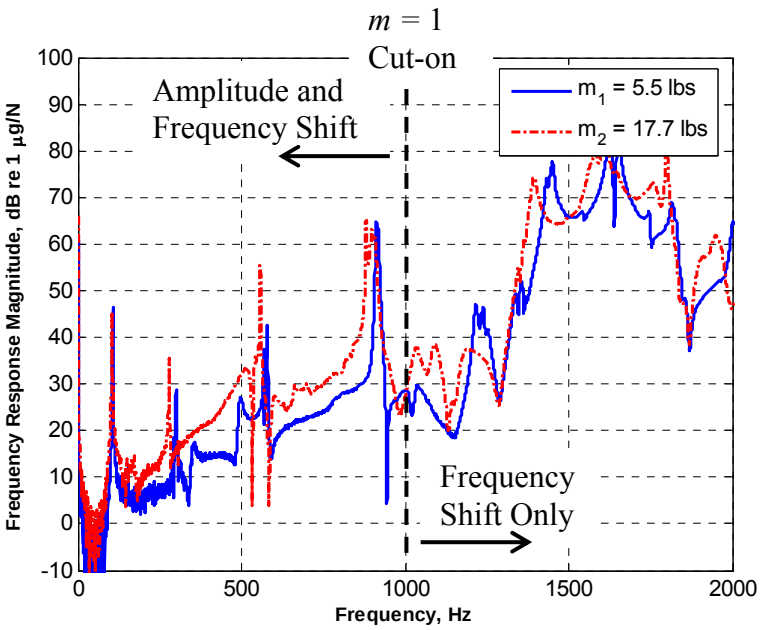

Figure 3-26: Frequency Response of the $n_r = +5$ Harmonic Due to a Force at $n_f = +2$ for Two Different Periodic Structure Masses

3.3 The Effect of A-Periodically Attached Masses

Data presented in the previous chapter dealt with a special case in which the structure attached to a cylindrical shell is periodic in nature. Often attached structure is found in non-periodic configurations. Two masses were added to the structure to allow for a comparison of the change in response characteristics for a-periodically attached structure relative to periodically attached structure.

Two 17.6lb (7.7kg) masses were attached to the shell and were positioned at the 215° and 295° angular locations. These masses were attached in the same manner as the masses were for the periodic test cases. Figure 3-27 compares the average frequency response function amplitude across the entire measurement range for the clean shell and the a-periodically distributed mass test cases. The force harmonic for both of these plots is $n_f = +2$. The direct response, at $n_r = +2$ is approximately equal for both cases. A sensor failed during the a-periodic test, so the measurement resolution of the array was decreased by ½ to maintain a uniform distribution. Comparison of the scattered harmonics between the two cases shows that increased energy is seen across all harmonics for the a-periodic case. Unlike the periodic test case where specific harmonics are excited, energy appears to be spread to all harmonics in the presence of a-periodic structure. Although an increase in response was seen at all harmonics, the response of the $n_r = 0$ and $n_r = -4$ did not appear to increase as much as the others. The reason for this was not discovered. However, it is noted that the response at these harmonics is lower relative to others in the clean shell test case as well.

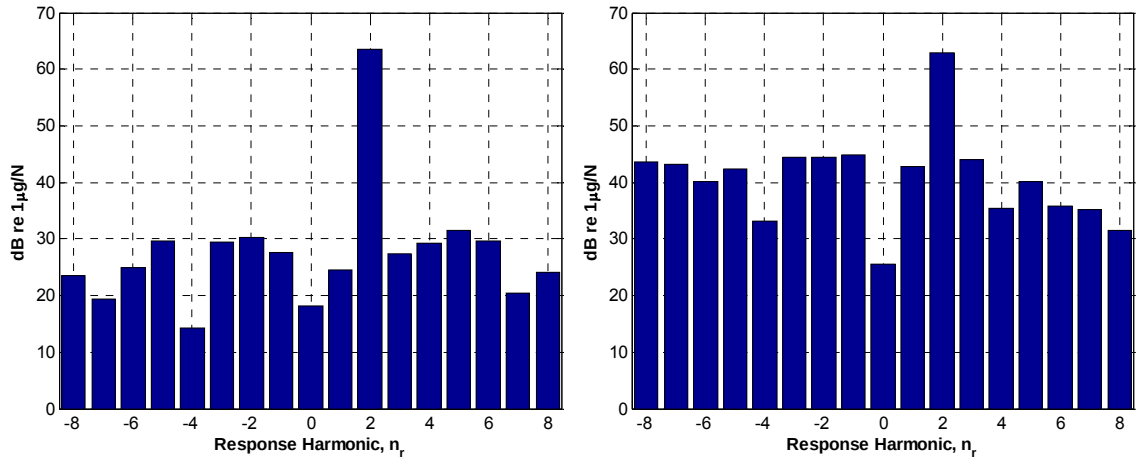

Figure 3-27: Average Frequency Response Magnitude (from 0-3200 Hz) to a Force Input at $n_f = +2$ for the clean shell *(left)*, and a-periodically attached mass *(right)* test cases.

Figure 3-28 show the frequency dependant nature of the response to the $n_f = +2$ force for harmonics from $n_r = -8$ to $+8$. This plot shows that energy is spread across both the frequency range and spatial harmonic range of the measurement.

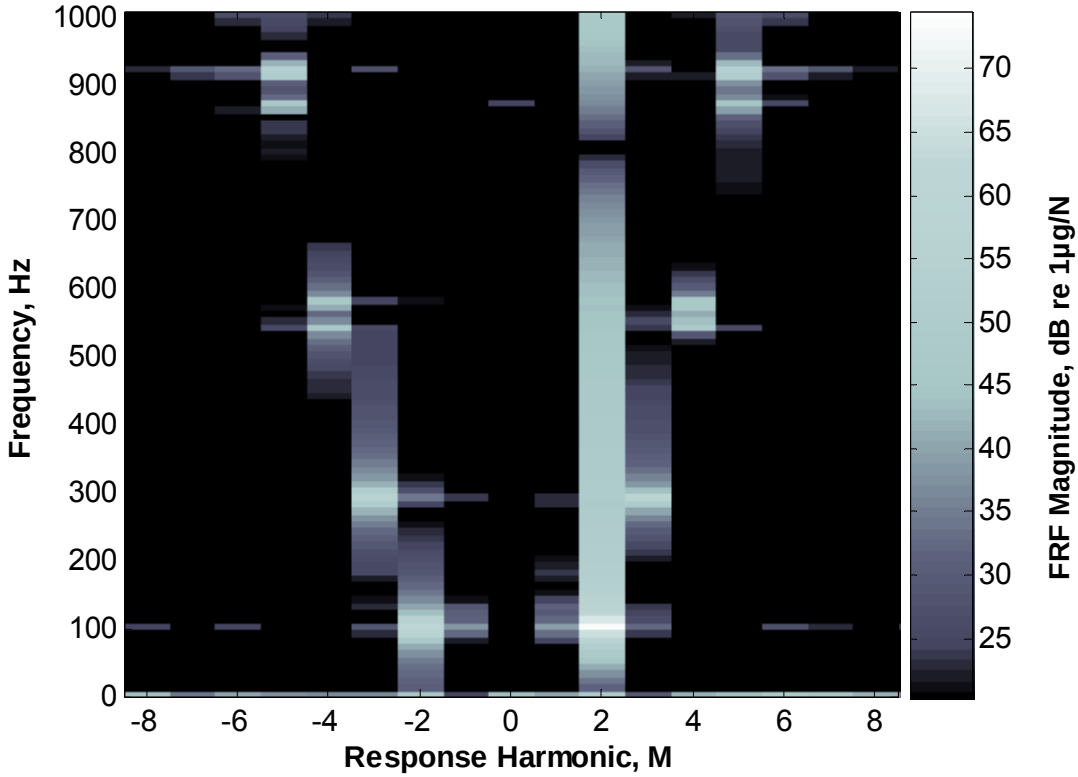

Figure 3-28: Frequency Response Magnitude for a Traveling Force Wave at n_f = +2 with 2 A-periodically Attached Masses

The change in scattering between the clean shell and a-periodically attached mass test cases was measured. Figure 3-29 shows the frequency and spatial harmonic dependency of this change in scattering. In the periodic test case, the change in scattering occurred at discrete spatial harmonics. In the a-periodic test case, the change in scattering appears to be spread more evenly across the spatial harmonics. Less change in scattering is noted relative to the periodic test case. Additionally, the change in scattering due to the addition of a-periodic masses appears to occur at discrete frequencies. This is contrary to the effect seen with a-periodic masses, in which a change in scattering was seen across a broad frequency range.

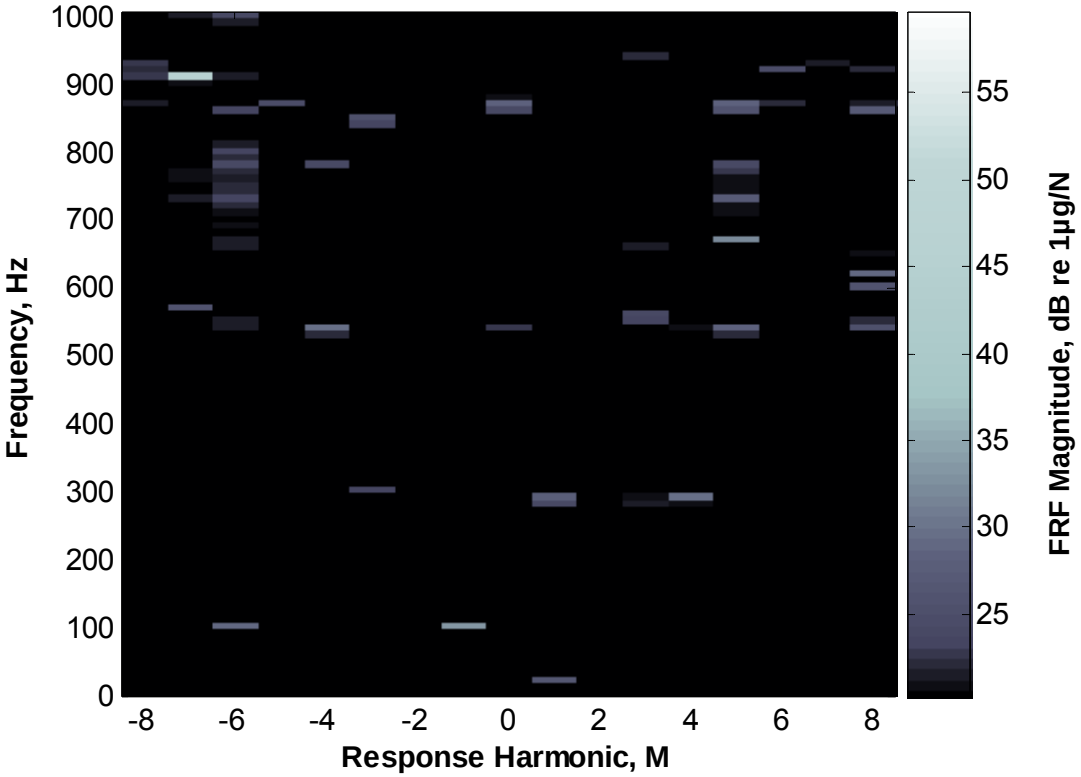

Figure 3-29: Change in Scattering Due to the Addition of 2 A-Periodically Attached Masses for a Traveling Force Wave at $n_f = +2$

Figure 3-30 plots the response of harmonics $n_r = +3$ through +7 for a force input at $n_f = +2$ for the a-periodic mass test case. A similar plot was created for the dominant response harmonics for the periodic test case (Figure 3-23). In contrast to the periodically distributed masses, the scattered response of none of the harmonics appears to follow the stiffness line of a mode. Instead, the scattered responses appear to increase rapidly near structural resonances. This behavior explains the discrete frequencies shown in Figure 3-29. The higher mobility (lower harmonic) modes appear to have more scattered energy in this frequency range than the higher order modes.

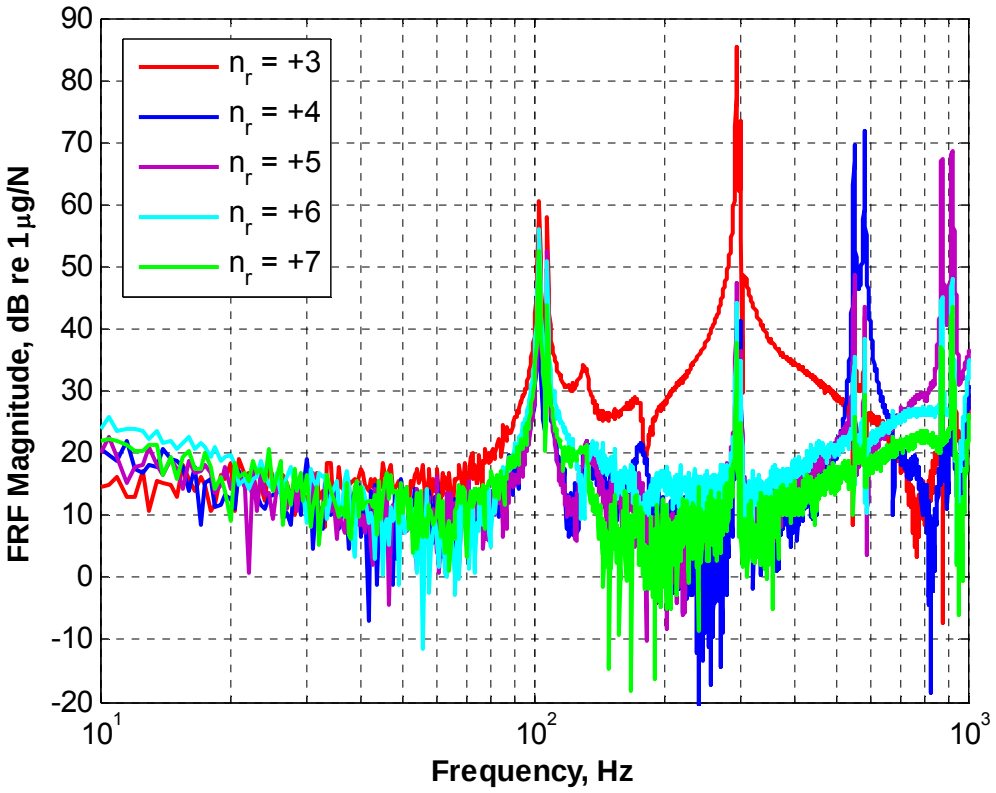

Figure 3-30: Scattered Response Harmonics to a Force Input at $n_f = +2$

Chapter 4

Summary and Conclusions

4.1 Summary

Ideal cylindrical structures with no discontinuities behave in a well defined manner and may be predicted with basic equations of motion. In practice, most cylindrical structures deviate from the behavior of the ideal structures due to the presence of impedance discontinuities. The experiment presented in this paper was designed to infer the changes in the response of the shell when masses were attached both periodically and a-periodically. Test data was taken by assembling a matrix of point responses to point forces. A data processing methodology was devised to allow for analysis of the structural response in terms of spatial harmonics of both t+he input force and response acceleration. The spatial harmonics were viewed in terms of both traveling wave and standing wave components.

Measurements performed on the clean shell (no added mass) demonstrated scattering characteristics. If the shell was truly uniform and had ideal boundary conditions, no scattering would be expected. Measured scattering in the clean shell is attributed to the weld seam in the pipe section, non-ideal boundary conditions, and potential errors in instrumentation calibration and placement.

The direct response characteristics (i.e. the response of harmonic n_r to a force at harmonic n_f, where $n_r = n_f$) were seen to change when periodically distributed masses

were attached to the structure. Specifically, the direct response at the harmonic equal to the number of attached masses was changed. Before adding masses, the direct response a traveling wave response of a mode with a single resonance frequency. After periodic masses were added, the direct response was split into two modes with separate resonance frequencies. These two modes responded as standing waves at resonance. The scattered response was found to increase at specific spatial harmonics related to the input force harmonic and the number of periodically attached masses. The scattered response at these harmonics appeared to follow a characteristic stiffness line in the stiffness dominated frequency range.

The amount of scattered energy was found to increase when the mass of the periodically attached structure was increased. The phenomena was observed only below the cut-on frequency of the m=1 modes (non-uniform axial variation).

When masses were attached to the structure in an a-periodic distribution, it was found that energy was scattered across a broad range of spatial harmonics. Unlike the periodic case, scattering appeared to occur primarily near resonance frequencies of the structure.

Observations on the scattering characteristics in cylindrical structures shown in this paper will help confirm behavior modeled in analytical and numerical models. The unexpected scattering shown in all test cases demonstrates that some scattering is likely present in most real cylindrical structures.

4.2 Future Work

The experiment presented in this paper identifies some of the basic scattering characteristics that may be present on real cylindrical structures. The experiment also demonstrates the ability to infer the forced response on a spatial harmonic basis with only point forces applied. This work could serve as a foundation for a more detailed exploration of scattering characteristics. Potential studies that could be performed are:

- The change in scattering characteristics to periodic and a-periodic stiffness discontinuities
- The change in scattering characteristics to periodically distributed structure of unequal mass or stiffness
- The combined scattering characteristics of two different types of discontinuities (e.g. periodic masses + aperiodic)

If these studies or others are performed experimentally, the author recommends changing the experimental setup from that presented in this paper. Since the weld seam is suspected to have caused undesired scattering, it is recommended that a continuous structure be used. Additionally, the support of the shell could be modified to decrease its effect on the scattering characteristics. Although this experiment focused only on the input and output relationship in the radial direction, the coupling of forces and responses in all three directions would be informative.

Finally, it is suggested that any test program be supplemented by sensitivity studies with computer models. The experimental procedure outlined in this paper requires a large amount of time input for a single set of data. Therefore, this test is more

appropriately suited as a confirmation of sensitivity studies performed numerically than as a primary sensitivity study test platform.

Bibliography

1) Blevins, R. 1995. *Formulas for Natural Frequency and Mode Shape.* Malabar, FL: Krieger Publishing Company.

2) Pray, C.M., and S.A. Hambric., "Finite Element Study of Harmonic Forcing Function Scattering Mechanisms for Cylindrical Structures." *Proceedings of IMECE2002*, November 2002.

3) Leissa, Arthur W. 1973. "Vibration of Shells" NASA SP-288, Washington D.C.

4) Feit, David, and M.C. Junger. 1993. *Sound Structures and their Interaction*, Acoustical Society of America.

5) Allaei, D., W. Soedel, and T.Y. Yang. 1987. "Eigenvalues of Rings with Radial Spring Attachments." *Journal of Sound and Vibration* 121(3), 547-561.

6) Wildheim, J. 1981. "Excitation of Rotating Circumferentially Periodic Structures." *Journal of Sound and Vibration* 75(3), 397-416.

7) Chang, J.Y and J.A. Wickert. 2001. "Response of Modulated Doublet Modes to Traveling Wave Excitation." *Journal of Sound and Vibration* 242(1), 69-83.

Appendix A

Sensitivity to Structural Damping

With the three periodic masses (17.7 lbs) attached to the shell, damping material was added to the structure. The damping was added by attaching rubber pads to the exterior circumference of the shell. Loosely fit nylon straps were used to hold the rubber pads in place. Figure A-1 compares the scattered response at the n_r = +2 harmonic to a force at the n_f = -4 harmonic for test cases with and without added damping. Figure A-2 also compares the scattered response for test cases with and without added damping. However, Figure A-2 shows the scattered response at the n_r = +5 harmonic to a force at the n_f = +2 harmonic. In both of these figures, the scattered response does not appear to change significantly away from resonance frequencies when damping is added to the structure. The scattered response decreases significantly at the resonance frequencies of the shell. The behavior is expected since the addition of damping to a system tends to reduce the magnitude of the response at resonance. The amount that the scattered response decreased with added damping at the resonance frequencies did not appear to occur in a predicable manner. Table A-1 compares the decrease in response of the direct terms ($n_r = n_f$) at each of the resonant frequencies to the decrease in response of scattered terms at the same frequencies. In some instances, the scattered response at a resonance frequency decreased significantly more than the direct response. This variability suggests that the addition of damping to a structure may not only decrease the responsiveness of a structure at its resonant frequencies, but influences the scattered response characteristics.

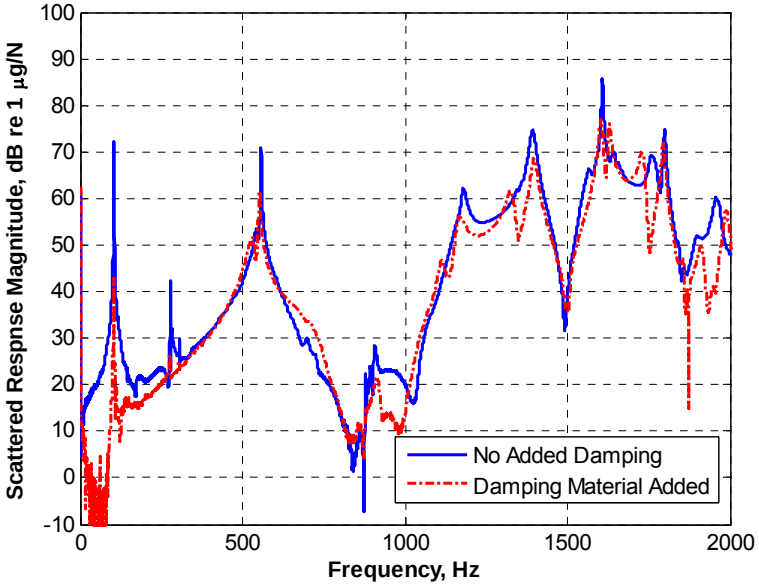

Figure A-1: Frequency Response of the n_r = +2 Harmonic Due to a Force at n_f = -4 With and Without the Structural Damping

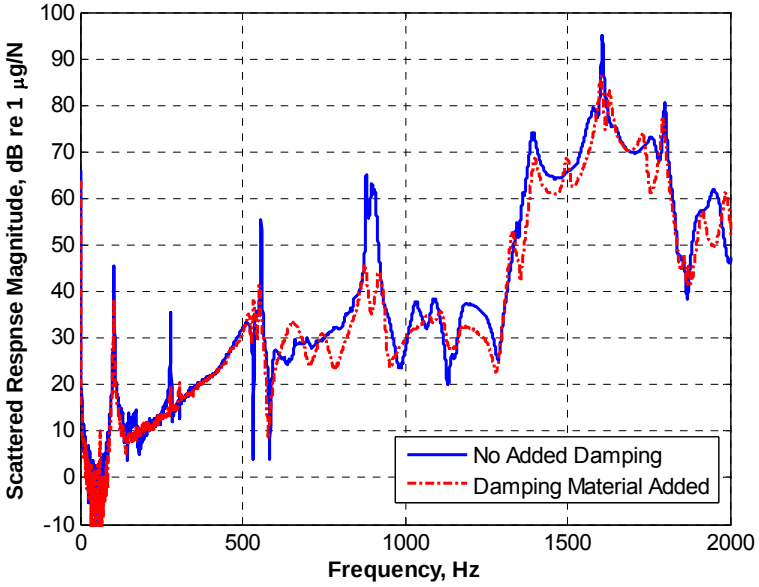

Figure A-2: Frequency Response of the n_r = +5 Harmonic Due to a Force at n_f = +2 With and Without the Structural Damping

Table A-1: Sensitivity of Scattering at Resonance to Added Damping

		Decrease in Response at Resonance, dB re 1μg/N					
Harmonic	**Frequency**	$n_f = n_r$	$n_f = 2$, $n_r = -1$	$n_f = 2$, $n_r = 5$	$n_f = -4$, $n_r = -1$	$n_f = -4$, $n_r = 2$	$n_f = -4$, $n_r = -7$
2	103	10.8	9.7	6.84	30.49	29.27	
3	277	4	2.1	15.86	10.24	15.74	22.456
3a	305	12.81	4.73	3.9	9.24	4.84	
4	552	9.02	11.47	14.26	9.05	9.26	7.93
5	878	12.81		19.26		6.85	